2013

Automatic Segmentation of Pressure Images Acquired in a Clinical Setting

Anathea Pepperl
Virginia Commonwealth University

Automatic Segmentation of Pressure Images Acquired in a Clinical Setting

A dissertation submitted in partial fulfillment of the requirements for the degree of Doctor of Philosophy at Virginia Commonwealth University.

by

Anathea Pepperl Bachelor of Science, Biomedical & Electrical Engineering
Rensselaer Polytechnic Institute
Director: Paul A. Wetzel, PhD
Associate Professor
Department of Biomedical Engineering

Virginia Commonwealth University
Richmond, Virginia
May 2013

Acknowledgements

I would like to thank my adviser, Dr. Paul A. Wetzel, for always being in my corner. The project is supported by a grant from the National Institute of Health R01NR010381, with Dr. Mary Jo Grap serving as PI, whose unflappable leadership really made this project possible. I'd also like to thank the entire Skin Integrity Backrest Elevation (SIBRE) Study team: Angela Parker, our project manager, for keeping us all motivated and organized; Lisa Sievers and Melissa Bucalan Rooney, for being wonderful nursing graduate students that not only asked the clinical questions but also did so much of the leg work needed to answer them; Dr. Christine Schubert, data nerd and statistics guru, for all of her support throughout this entire process; Ruth Burk and Patrick Headley, who were absolutely instrumental to the early phases of this project; Dr. Cindy Munro who actively supported our work, even after her move to sunny Florida, and kept us curious. I'd also like to thank all of the research assistants, Kin Choi, Elizabeth Butler, Hadja Diallo, Camille Richards, Brittany Russell, Jessica Schumacher, for all of their hard work enrolling patients and collecting data in the ICU.

I would also like to thank the rest of my committee members: Dr. Ou Bai, for your jovial nature and for your belief in me; Dr. Jennifer Wayne, for being a great female academic role model for me; and Dr. Najarian, for being my image analysis expert.

I am so very grateful to all the VCU students who have made this journey memorable, especially Dr. Pallavi Ramnairan, Nyimas Hajjah Isti Arief, and Dr. Colleen McLoughlin for being my support system. I'd also like to thank the students of Engineers Without Borders, especially Allison Yaguchi and Chris Holden, for the healthy distractions from research.

Finally, I'd like to thank all of my friends and family for their continued support. To my wonderful parents, I thank you for shaping me into the person that I am, and to my amazing siblings, I thank you for giving me the chance to shape the persons you will become. Most of all, I thank my husband, Kevin Pepperl, who has supported me throughout this entire journey with patience and his own special sense of humor.

Contents

List of Figures **vi**

List of Tables **viii**

Abstract **ix**

1 Introduction **1**

1.1 Overview 1

1.2 Pressure Ulcers in the Critically Ill 3

1.2.1 Intrinsic Factors 5

1.2.2 Extrinsic Factors 7

1.2.3 The Pressure-Time Curve 8

1.3 Pressure Mapping Systems 10

1.4 Research Objective 12

1.5 Outline of Following Dissertation 13

2 Human Motion Analysis Literature Review **14**

2.1 Human Motion Analysis Functional Structure 14

2.2 Human Detection 15

2.2.1 Generative vs Discriminative Approaches 15

2.2.2 2D vs 3D Approaches 16

2.2.3 Kinematic vs Shape Models 17

2.3 Image Features 18
2.3.1 Dense vs. Sparse Features 18
2.3.2 Commonly Used Features 19
2.4 Discussion 22

3 Data Acquisition **23**
3.1 Hardware 23
3.1.1 XSensor Pressure Imaging System 23
3.1.2 Inclinometer 24
3.1.3 Actigraphy 24
3.2 Software 25
3.2.1 Data Synchronization 25
3.2.2 Pressure Image Preprocessing 25

4 Pose Classification Algorithm **28**
4.1 Introduction 28
4.2 Materials and Methods 29
4.2.1 Data 29
4.2.2 Potential Features 30
4.2.3 Feature Selection 31
4.2.4 Classification Techniques 31
4.3 Results 34
4.4 Discussion 35

5 Segmentation Algorithm **37**
5.1 Introduction 37
5.2 The Model 38
5.3 Preprocessing 41
5.4 Pose Optimization 41

5.4.1 Finding Extremities . . . 41
5.4.2 Sampling Procedure . . . 42
5.4.3 Cost Function Minimization . . . 42
5.4.4 Image Cost Function . . . 43
5.5 Determining Regions of Interest . . . 45
5.6 Experimental Results . . . 45
5.7 Conclusion . . . 50

6 Role of Self-Positioning **55**
6.1 Introduction . . . 55
6.2 Methods . . . 56
6.2.1 Sample and Setting . . . 56
6.2.2 Procedures . . . 56
6.2.3 Data Analysis . . . 57
6.3 Results . . . 58
6.3.1 Participants . . . 58
6.3.2 Peak Pressure . . . 58
6.3.3 Average Pressure . . . 59
6.3.4 Additional Findings . . . 60
6.4 Discussion . . . 60

7 Conclusions **65**
7.1 Summary . . . 65
7.2 Future Work . . . 66

A Ellipses **82**
A.1 Fitting an Ellipse to a Set of Boundary Points . . . 84

B Nelder-Mead Simplex Algorithm **85**

List of Figures

1.1 Common anatomical sites of pressure ulcers 2

1.2 NPUAP Pressure Ulcer Staging System 4

1.3 Comparison of conceptual schemas 5

1.4 Comparison of pressure time curves 11

3.1 Data Acquisition Flow Diagram 25

3.2 Signal Processing Flow Diagram 26

3.3 Artifact Removal 27

4.1 Pose Classification 30

4.2 Pose Classification Neural Network 32

4.3 Pose Classification Tree 35

4.4 Results of Pose Classification Methods 36

5.1 Previous segmentation attempts 39

5.2 Articulated model 40

5.3 Image Cost Function 44

5.4 Manual Segmentation App 46

5.5 Comparison of Automatic Segmentation - Left Lateral 48

5.6 Comparison of Automatic Segmentation - Supine(1) 49

5.7 Comparison of Automatic Segmentation - Supine(2) 50

5.8 Comparison of Automatic Segmentation - Supine(3) 51

5.9 Comparison of Automatic Segmentation - Right Lateral 52

6.1 Effect of backrest elevation on peak pressure 63

6.2 Effect of Body Mass Index (BMI) on peak pressure 64

List of Tables

1.1 NPUAP Pressure Ulcer Staging System 3

2.1 Examples of Generative and Discriminative Models 17

3.1 Data collection schedule 23

4.1 Comparison of Pose Classification Models 36

5.1 Normal Values for Range of Motion of Joints 43

5.2 Segmentation Results 47

6.1 Demographic Data of Repositioning Study Participants 58

Abstract

AUTOMATIC SEGMENTATION OF PRESSURE IMAGES ACQUIRED IN A CLINICAL SETTING

By Anathea Pepperl, Ph.D.

A dissertation submitted in partial fulfillment of the requirements of the degree of Doctor of Philosophy at Virginia Commonwealth University.

Virginia Commonwealth University, 2013.

Major Director: Paul A. Wetzel, Ph.D.

Associate Professor, Dept. Biomedical Engineering

Hospital-acquired pressure ulcers are a major health care concern, costing the United States approximately $3 billion per year. Development of a pressure ulcer prolongs hospital length of stay by almost 4 days and increases mortality by more than 7%. Despite the apparent need for pressure ulcer prevention, the incidence of pressure ulcers has increased almost six times more than the increase in total number of hospitalizations.

One of the major obstacles to pressure ulcer research is the difficulty in accurately measuring mechanical loading of specific anatomical sites. A human motion analysis system capable of automatically segmenting a patient's body into high-risk areas can greatly improve the ability of researchers and clinicians to understand how pressure ulcers develop in a hospital environment. Such a system could also reduce costs associated with patient care and aid in clinical intervention decision-making, such as

determining an effective turning schedule or selecting appropriate support surfaces.

This project has developed automated computational methods and algorithms to analyze pressure images acquired in a hospital setting. The first step of this algorithm involves the correct classification of pressure images into appropriate pose classes (left lateral, supine, and right lateral). The classification algorithm achieved 99% overall accuracy. The second step of this algorithm uses a kinematic model to estimate the overall pose of the patient. From the model, high risk areas were extrapolated. The algorithm accuracy depended on the body site, with the sacrum, left trochanter, and right trochanter achieving an accuracy of 87-93%.

This project represents the first algorithm to reliably segment pressure images into high-risk regions of interest, given a variety of poses that patients generally take. The proposed algorithm generates a statistical summary of each region, allowing clinicians to study how pressure ulcers may develop in a clinical setting.

Chapter 1

Introduction

This chapter demonstrates the need for further research in pressure ulcer epidemiology, particularly as to how progression occurs in the critically ill. First, intrinsic and extrinsic factors are discussed, followed by a review of the pressure sensing systems currently available. Lastly, this chapter summarizes the overall research objective and the method proposed in this project.

1.1 Overview

In the United States, pressure ulcers developed in hospitals affect more than 1.5 million patients and represent an annual cost of $2.2 to $3.6 billion [1]. Pressure ulcer incidence studies vary greatly, reporting anywhere from 4% – 49% of patients in a hospital setting develop pressure ulcers [2, 3, 4].

According to the Healthcare Cost and Utilization Project (HCUP) [5] report, in 2006 there were 503,300 hospital stays during which pressure ulcers were noted. This is a 78.9% increase from 1993 where there were about 281,300 pressure ulcer related hospitalizations. During this same time period, the total number of hospitalizations increased by only 15%. The National Quality Forum argues that pressure ulcers that develop while hospitalized are preventable with implementation of evidence-based guidelines [6]. However, the discrepancy

between this statement and the lack of improvement in pressure ulcer incidence rates points to a gap in our understanding of pressure ulcer risk.

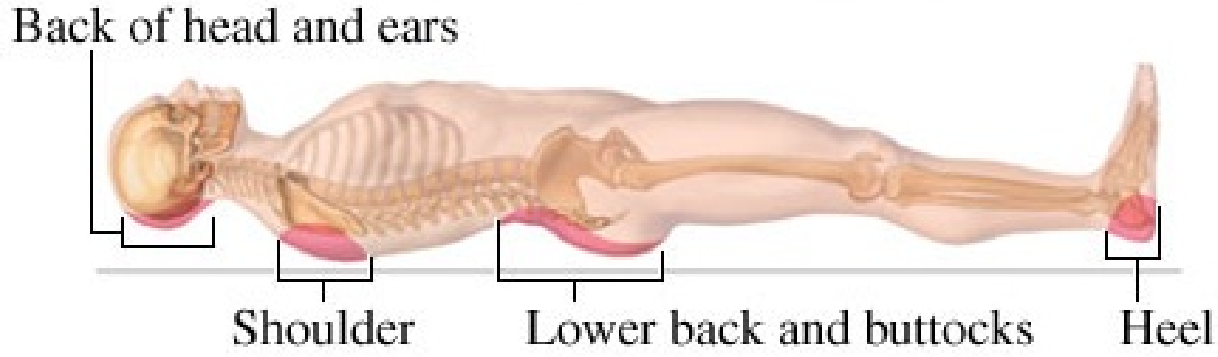

Figure 1.1: Common anatomical sites of pressure ulcers. Adapted from [7].

Prolonged pressure is certainly a crucial factor in the development of a pressure ulcer. The weight of the body causes a compressive load on the muscle and skin over the bony prominences – such as the sacrum, scapula, or calcanae – resulting in tissue death and necrosis[8, 9]. Figure 1.1 shows the areas deemed at-risk of developing pressure ulcers, particularly for those who are confined to a hospital bed. However, there exists two conflicting theories (the deep tissue injury and top–to–bottom models) as to how external pressure translates to tissue injury. The deep tissue injury model claims that ulcers begin at the muscle layer near a bony prominence, eventually growing outward until injury is seen at the epidermis. The top–to–bottom model claims that tissue injury first occurs at the epidermal layer and proceeds inward. The deep tissue injury has gained more recent attention, particularly with the fact that muscle cells are more susceptible to tissue injury [10]. Still, according to the most recent international survey on pressure ulcer prevalence, of the 6,859 facility–acquired pressure ulcers reported, 4,985 (76%) were Stage I or Stage II superficial (skin) ulcers[11] while only 642 (10%) were suspected deep tissue injury (DTI). Figure 1.2 illustrates the differences in each of the pressure ulcer stages, as defined by the National

Pressure Ulcer Advisory Panel (NPUAP).[1] Since this study is concerned with pressure ulcer development in the critically ill, this higher occurrence of superficial pressure ulcer shows that the top–to–bottom model is likely the more relevant theory in this research project.

Stage	Description
Stage I	Intact skin with non-blanchable redness of a localized area, usually over a bony prominence.
Stage II	Partial thickness loss of dermis presenting as a shallow open ulcer with a red pink wound bed, without slough.
Stage III	Full thickness tissue loss. Subcutaneous fat may be visible but bone, tendon or muscle are not exposed. Slough may be present but does not obscure the depth of tissue loss.
Stage IV	Full thickness tissue loss with exposed bone, tendon or muscle. Slough or eschar may be present on some parts of the wound bed.
Unstageable	Full thickness tissue loss in which the base of the ulcer is covered by slough and/or eschar in the wound bed.
Suspected Deep Tissue Injury	Purple or maroon localized area of discolored intact skin or blood-filled blister due to damage of underlying soft tissue from pressure and/or shear. The area may be preceded by tissue that is painful, firm, mushy, boggy, warmer or cooler as compared to adjacent tissue.

Table 1.1: NPUAP Pressure Ulcer Staging System

1.2 Pressure Ulcers in the Critically Ill

Patients who are critically ill are especially susceptible to pressure ulcers for a number of intrinsic and extrinsic factors. Braden & Bergstrom developed a conceptual schema to relate

[1]While the results of the 2008 – 2009 International Pressure Ulcer Prevalence Survey™demonstrates that facility–acquired pressure ulcers are largely superficial skin ulcers, it is important to note that the classification "suspected deep tissue injury" was formally introduced to the pressure ulcer staging system recently[12]. As such, its low incidence may be somewhat attributed to unfamiliarity of hospital staff in classifying a pressure ulcer as a suspected deep tissue injury. However, the fact still remains that the majority of facility–acquired pressure ulcers at any given time are described by tissue injury that starts at the epidermal layer.

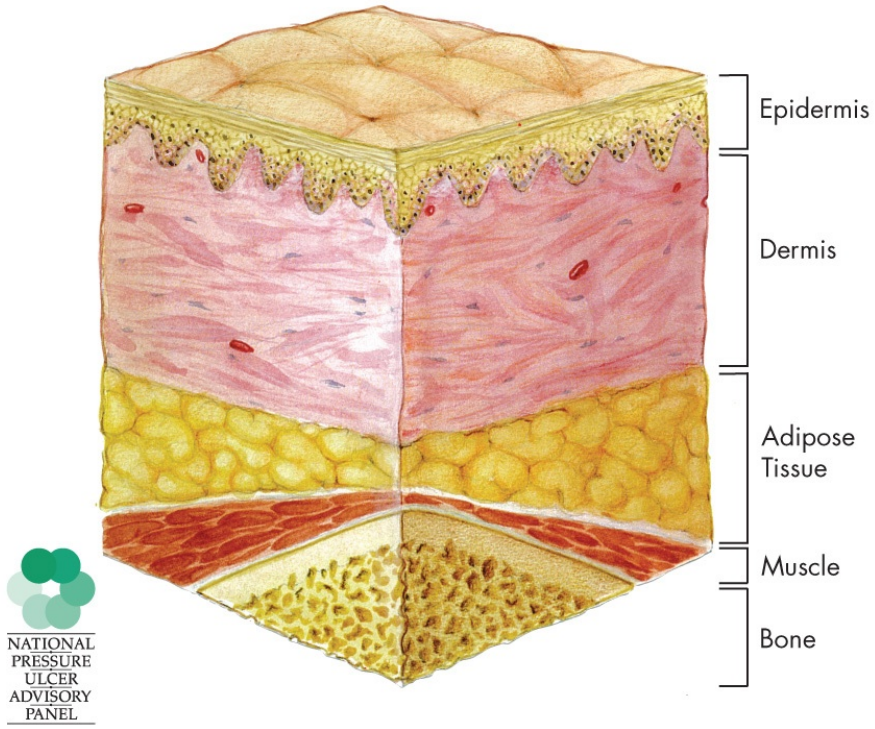

(a) Normal skin

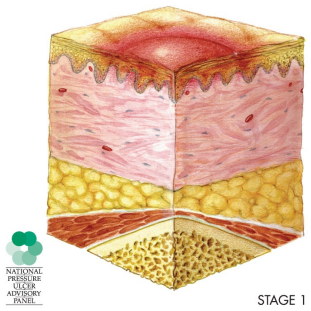

(b) Stage 1

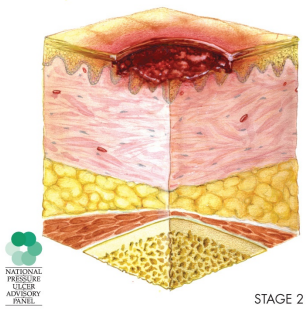

(c) Stage 2

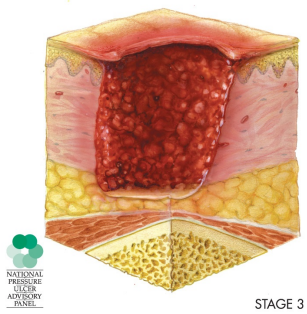

(d) Stage 3

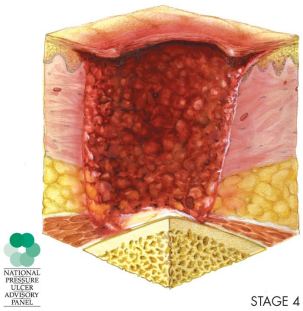

(e) Stage 4

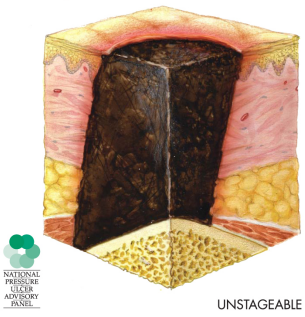

(f) Unstageable

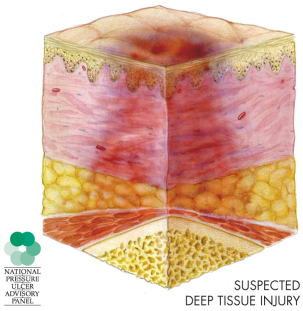

(g) Suspected DTI

Figure 1.2: National Pressure Ulcer Advisory Panel's Staging System. [13]

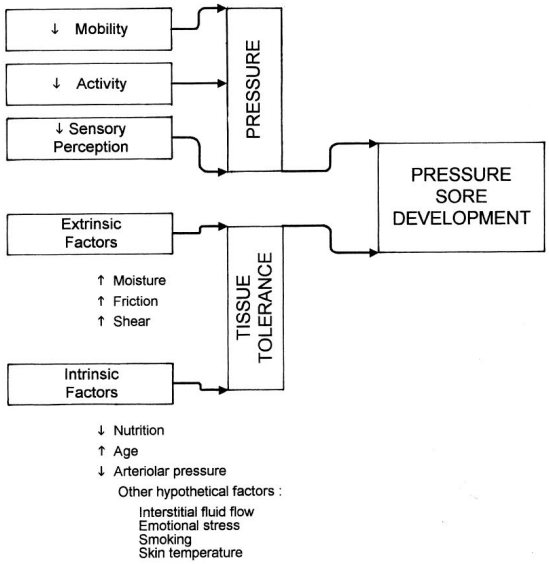

(a) Braden and Bergstrom (1987)

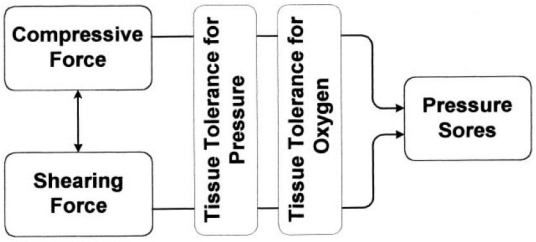

(b) Defloor (1999)

Figure 1.3: Comparison of conceptual schemas. Reprinted from Defloor [15]

these intrinsic and extrinsic factors to a conceptual model of tissue tolerance[14]. They theorized pressure ulcers were caused by pressure and tissue tolerance.

Defloor later adapted this model[15], citing that tissue tolerance alone cannot cause pressure sores. Rather, a sufficiently high pressure sustained for a sufficiently long time will cause pressure sores. An individual's tissue tolerance will dictate the maximum threshold for pressure intensity and duration required to cause tissue injury. Figure 1.3 provides a visual representation of the two conceptual schemas. Tissue tolerance for pressure is influenced by both extrinsic and intrinsic factors. This section will outline the various intrinsic factors that make critically ill patients particularly susceptible to pressure ulcers.

1.2.1 Intrinsic Factors

Intrinsic factors refers to patient-specific characteristics that might make that person more vulnerable to developing pressure ulcers. Many authors have attempted to identify these intrinsic factors that predispose certain patient populations to develop pressure ulcers; their research has led to the development of various risk assessment tools for use in clinical prac-

tice [14, 16, 17, 18, 19, 20].

Determining which risk factors are most important is a difficult task; in a review of 100 articles by Gosnell [21], 126 different items documented as risk factors for pressure ulcer development were found. However, there are several factors that have been consistently named as major determinants of pressure ulcer susceptibility, namely mobility, age, and nutrition.

Mobility

Mobility is associated with two concerns: the individual's ability to feel pain or discomfort and the individual's physical ability to reposition themselves in response to the painful stimulus. Healthy individuals regularly change their position in order to relieve pressure.

Keane [22] observed that normal sleeping individuals make an average of one gross postural change every 11.6 minutes, suggesting that this is the minimum physiological mobility required in order to maintain healthy tissue. When a patient is unable to perform a postural change, interface pressures must be relieved, either through manual turning or the use of pressure-relieving devices. Indeed, much of the costs associated with pressure ulcer prevention revolves around the use of equipment intended to reduce interface pressures caused by prolonged periods of immobility.

Exton-Smith and Sherwin [23] demonstrated the importance of spontaneous movement when they counted elderly individuals' spontaneous movements during sleep. In their study, patients who made 50 or more movements during the 7-hour observation period had no pressure ulcers. In comparison, 90% of patients who made 20 or fewer movements developed ulcers.

Papanikolaou et al. [24] found that patients with reduced mobility were at greater risk of pressure ulcer than those without reduced mobility. Similarly, Mino et al. [25] found that patients who are unable to turn over in bed are four times more likely to develop pressure ulcers than those patients who are capable of turning in bed.

Age

As individuals age, their skin experiences a number of pathological changes. These changes alter the elastin and collagen composition of the skin, reducing skin elasticity and ultimately reducing the skin's tolerance to pressure [15].

Margolis et al. [26] found a statistically significant relationship between the likelihood of pressure ulcer development and increased age. In the US, a study of 116 acute care facilities [27] found that 73% of pressure ulcers developed in those over 65 years of age.

While age is a major factor in pressure ulcer development, clinicians should be cautioned that individuals of any age can develop a pressure ulcer depending on their condition [28].

Nutrition

The exact influence of nutrition on tissue tolerance, and therefore pressure ulcer development, is still not well understood [29]. However, compromised nutritional status, such as rapid weight loss, undernutrition, protein energy malnutrition (PEM), and dehydration, has been linked to pressure ulcer development [30, 31]. Other nutrition-related risk factors associated with increased risk of pressure ulcers include low body mass index (BMI), reduced food intake, and impaired ability to eat independently [32, 33].

Although the exact mechanism by which nutrition affects pressure ulcer development is unknown, it is reasonable to assume that nutrition may impact an individual's ability to withstand the adverse effects of pressure shear and friction.

1.2.2 Extrinsic Factors

Pressure, shear, and friction play the key role in causing pressure ulcers. The role of pressure is so vital to the understanding of pressure ulcers that it will be discussed in greater detail in the next section. Shear and friction are forces that may exacerbate the impact of pressure, resulting in greater tissue damage.

Shear Forces

Shear is a mechanical stress that is parallel to a plane of interest. When the head of the bed is elevated, it is thought that shear develops as a result of the patient's sacral skin adhering to the bed linen. If the effects of shear are prolonged or exacerbated by the presence of moisture, localized stretching of the microcirculation of the skin may occur.

With a sufficient shear force, the amplitude of external pressure needed to occlude the underlying microvasculature is reduced by about half of that required when there is no shear present [34].

Shear is difficult to study in isolation as it is difficult to apply pressure without causing shear, or to apply shear without creating compressive force [35].

Friction

The role of friction in pressure ulcer development is not well understood, owing in part to inconsistent terminology in the literature and failure to identify the use of static or dynamic friction[36]. One of the earliest authors to study friction and pressure ulcer development was published Dinsdale in 1974[37]. His study used a swine model to apply friction and a compressive load; however, it is unclear if friction applied was static or dynamic.

Dynamic friction is thought to exacerbate tissue injury of broken epidermis, or cause an initial break in the skin. Thus, while friction itself is not a primary factor[2] in the development of pressure ulcers, friction can accelerate tissue injury or delay wound healing.

1.2.3 The Pressure-Time Curve

Both the intensity and duration of a compressive load must be taken into account when investigating the role of pressure in the development of pressure sores. Several animal models and clinical research studies have attempted to describe the relationship between the intensity

[2]Not all friction injuries should be labeled as pressure ulcers. If tissue injury is caused solely by friction, the injury presents as a visible skin impairment, such as a skin tear or laceration. If, however, the injury presents as a blister with surrounding purple or maroon discoloration, then a pressure ulcer may be suspected.

and duration of pressure that can be tolerated without resulting in tissue injury. It is generally agreed that a parabolic relationship exists between the intensity and duration of pressure. In other words, while it is possible for tissue to be exposed to a low pressure for a longer duration without experiencing injury, it is also possible for a high intensity of pressure applied for only a short period of time to fail to produce tissue injury.

The relationship between intensity and duration was first evidenced in 1942, when Groth[38] analyzed the histological samples of ulcers produced in the gluteus muscle of rabbits. In the study, he observed that damage to muscle fibers and capillaries increased with the magnitude and duration of the mechanical loads applied. In 1953, Husain[39] applied mechanical loads of differing intensity and duration to rats; then sacrificed the animals 24 hours after the initial injury and studied histological samples of the affected areas. He noted that microscopic changes occur following a pressure of 100 mmHg applied for two hours, indicating that this might be the injury threshold for skeletal muscle. In 1959, Kosiak[40] used a dog model for pressure ulcers, illustrating an inverse trend between the magnitude and duration of pressures necessary before tissue injury occurred. Figure 1.4a includes the raw data Kosiak used to arrive at his conclusions, in which the symbol $\times$ indicated that ulceration occurred and the symbol $\bullet$ indicated that no ulceration was present. Finally, in 1976, Reswick and Rogers [41] developed an intensity-duration curve based on more than 980 observations in the Rancho Los Amigos hospital.

While Reswick and Rogers's pressure-time curve is often cited, it has fallen under scrutiny in recent years. Gefen (2009) [42] highlights the flaws associated with the simple pressure-time curve first hypothesized by Reswick and Rogers, pointing to the fact that the curve cannot be easily applied when pressure is applied for very short or very long periods. For example, patients undergoing a lengthy surgery of 12 hours or more could expect signs of ulceration at pressures lower than 25 mmHg. A study of four operating table surfaces by Defloor et al. [43] showed that none of the mattresses evaluated were able to reduce pressure below that threshold; and yet the majority of patients undergoing long periods of surgery do

not develop pressure ulcers [44]. Gefen proposed a sigmoid function to describe the pressure-time relationship. He defined the limit on the left-side of the curve using the work of Linder-Ganz et al. [45], which referred to pressures applied directly to muscle tissue. The limit on the right-side of the curve was found using the work of Gefen et al.[46], from which relative deformations in the muscle tissue were determined. The importance of Gefen's sigmoid function is that it provides a separate maximum intensity threshold (in which tissue injury will occur regardless of the duration), as well as a maximum duration threshold (meaning tissue injury will occur if a minimum pressure is sustained for an intolerable amount of time). Figure 1.4 illustrates how pivotal studies have changed clinical perceptions regarding the pressure-time curve.

A pressure higher than the capillary pressure slows the flow in the capillaries and lymph nodes, resulting in insufficient supply of oxygen and nutrients and insufficient evacuation of metabolic wastes.

1.3 Pressure Mapping Systems

Several instruments for analyzing pressure at the skin-bed interface exist. The most commonly used sensors for measuring interface pressures consist of two layers of a flexible material which have either conductive or capacitive electrodes embedded in a specific pattern. On one layer, electrodes form a column pattern and in the other layer, electrodes form a row pattern. The intersection of each row and column represents a unique sensing cell, typically called a sensel. Research has supported the validity of these sensors, manufactured by Tekscan (Tekscan, Inc.; Boston, MA) [49, 50] and XSensor (XSENSOR Technology Corporation: Calgary, Alberta, CANADA) [51, 52, 53].

A fiber-optic tactile sensor (KINOTEX sensor; NITTA Corp, Osaka, Japan) has also been shown to be a valid instrument for measurement of interface pressures [54]. This sensor is comprised of urethane foam which acts as a scattered medium, optical fiber as an

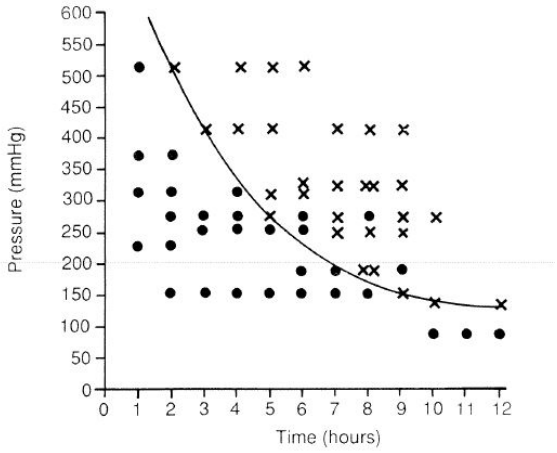

(a) Kosiak(1959)

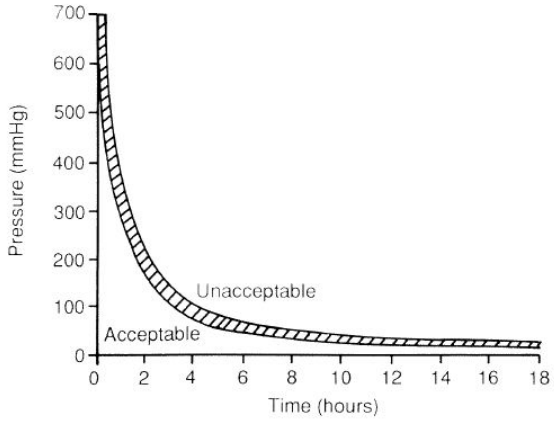

(b) Reswick & Rogers (1976)

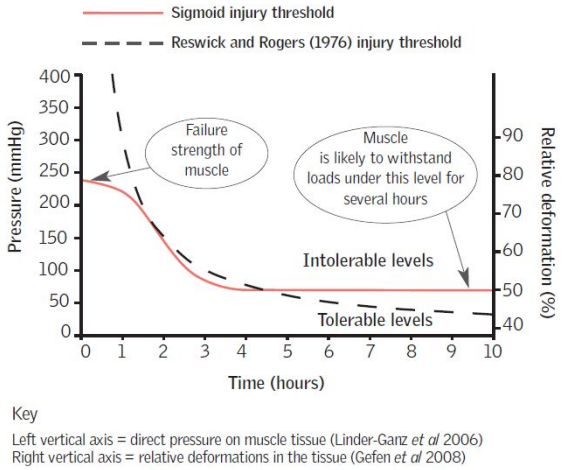

(c) Gefen (2009)

Figure 1.4: A comparison of pressure time curves. (a) and (b) Reprinted from Sacks [47]. (c) Reprinted from Gefen [48]

illumination source and energy detector, and optical receiver and a transducer. The sensor operates on the principle that deformation of the scattered medium results in a localized change to the illumination energy intensity.

Other studies have observed surface pressure and shear forces by attaching sensors directly to the skin of subjects [55]. Due to the critical condition of the subject population and the observation time, this method is deemed too invasive for use in the subject population.

While several studies have utilized sensors to measure pressure at the skin-surface interface, it is important to note that the majority of these studies can be placed into one

of two categories: (1) studies of healthy individuals; or (2) studies of stable patients with paraplegia. Few studies involve measuring the interface pressures experienced by hospitalized patients for an extended period of time and, to date, the author has found only one study [54] that monitored the interface pressures of 30 postoperative patients continuously for up to 48 hours.

1.4 Research Objective

One of the major obstacles to pressure ulcer research is the difficulty in accurately measuring mechanical loading of specific anatomical sites. It is because of this that much of the current research focuses on mechanical loading of a specific area, namely the sacrum, or summarize pressure statistics based on pressure across the whole body. However, hospital-acquired pressure ulcers also develop on the heel, scapula, and trochanter of patients.

The aim of this research project is to develop an algorithm for the segmentation of full-body pressure images acquired from the XSensor pressure sensing system into anatomical sites that are highly susceptible to pressure ulcers, or regions of interest (ROIs). The proposed system must be robust enough to account for various poses[3] that patients may assume in a clinical setting. The system will allow clinicians and researchers to extract information necessary to guide clinical intervention decisions and to further improve understanding of how pressure ulcers develop in a hospital setting.

This project also demonstrates the need for studying interface pressure over specific body sites in a controlled experiment used to evaluate the effects of a major risk factor on pressure ulcer development. Because immobility has long been considered a risk factor, but has rarely been studied in isolation, the project focuses on the role that immobility has on interface pressure, as measured in whole body scans and at different body sites.

[3]Here, "pose" is used in lieu of "position" to describe the particular way a patient is lying in bed. While the term "position" is more widely used in nursing research, the term "pose" is more commonly used in the field of computer vision. Additionally, "position" conveys a specific location on the coordinate axes, whereas "pose" conveys a kinematic description in the sense that body parts and joints are described in relation to one another.

1.5 Outline of Following Dissertation

The following dissertation is organized as follows. Chapter 2 provides an overview of human motion analysis[4], providing a comparison between bottom-up and top-down approaches. Chapter 3 gives a description of the hardware and software involved in collecting pressure images in a clinical setting. Chapter 4 gives detailed information as to how the patient pose was determined based on the acquired pressure images. Chapter 5 provides the pose estimation algorithm, which segments the pressure images into various regions of interest. Chapter 6 describes one application using segmented pressure images in order to better understand an important clinical factor in pressure ulcer development. Lastly, Chapter 7 provides general conclusions about the proposed research and its contributions to the field.

[4]Motion analysis and movement analysis may be used interchangeably throughout the literature. Here, motion analysis is used as it tends to be used in the field of computer vision; movement analysis tends to be used in the field of biomechanics.

Chapter 2

Human Motion Analysis Literature Review

This chapter discusses the broad topic of human motion analysis. Methodologies deemed appropriate for the proposed aims of this research project are identified. Finally, design considerations for the proposed system, which will be used to segment acquired pressure images into areas deemed high-risk for pressure ulcer development, are outlined.

2.1 Human Motion Analysis Functional Structure

Human motion analysis is currently one of the most active areas of research in the field of computer vision, and has many applications, including surveillance, medicine, sports rehabilitiation, video gaming, and human-computer interaction. The field of human motion analysis can be divided into three areas of focus based on their function: human detection, tracking, and activity recognition.[1] Human detection involves extracting the object of interest (here, the human body) from a scene. Depending on the application, human detection

[1]Several of the comprehensive surveys referenced in this section may divide the functional structure slightly differently. Aggarwal & Cai[56] divide human motion analysis into body structure analysis, tracking, and recognition. Moeslund & Granum [57] use four areas to describe the functional structure: initialization, tracking, pose estimation, and recognition. However, the categories can still more or less be fit into the three listed here.

may also include the labeling of human body parts, during which the human body is divided into segments connected by joints. Tracking involves finding feature correspondences between either the whole body or body segments in order to locate them in consecutive frames. Activity recognition analyzes the pose over time in order to categorize the actions performed by the subject. While there exists overlap between these three areas, this classification system provides a good framework by which to understand the field of human motion analysis. Given the scope of the proposed research project, the area of human detection and the associated task of segmenting the detected body into meaningful body parts is of the most interest.

2.2 Human Detection

Human detection is a broad field and there are various ways of classifying the different methodologies that exist. Gavrilla[58] chose to divide the subject into three parts: 2D approaches without explicit shape models, 2D approaches with explicit shape models, and 3D approaches. Aggarwal & Cai [56] provided a broader classification scheme, dividing instead between model-based and non-model-based approaches, and then making further classifications within the two groups. Poppe [59] also chose to divide the area into two main subjects: model-based (or generative) and model-free (or discriminative).

2.2.1 Generative vs Discriminative Approaches

Generative approaches employ Bayes' rule in order to create a full probabilistic model of all parameters. Generative, or model-based, approaches employ *a priori* information about the human body. Generative approaches consist of a modeling phase and an estimation phase. The modeling phase requires constructing a model that can be described using a finite set of parameters in order to model the body configuration, body shape, and appearance. The estimation phase involves finding the set of parameters that best fits the model to the ob-

served image. The complexity of the estimation phase depends on the number of parameters used to describe the model. When fewer model parameters are used, it is generally easier to converge to a solution; however, if not enough parameters are used, the solution may not adequately describe the image.

Within the general field of machine learning, discriminative models seek to model the conditional probability distribution $P(y|x)$ in order to predict y from x. Discriminative, or model-free, approaches do not assume *a priori* information about the human body. Instead, model-free approaches seek to describe human movement using simple low-level 2D features. Techniques using a model-free approach typically divide the image by superimposing a grid over the region of interest. Within each tile, a simple feature is computed. Features that have been used include: the sum of normal flow[60], the count of foreground pixels[61], and either color or pixel intensity[62]. The computed features are then assembled to form a feature vector, which is used to describe the state of movement over time.

The main difference between generative and discriminative methods lies in whether or not the probability distribution of the chosen image features is modeled (generative) or not modeled (discriminative). Generative and discriminative models have very different characteristics and the decision to use one versus the other is largely application-dependent. Model-free approaches do not suffer from initialization problems, as model-based approaches do. However, model-free approaches typically experience problems in dealing with self-occlusion. Additionally, the computed features must be able to generalize well over the invariant parameters and distinguish well between the variant ones. Examples of generative and discriminative models are listed in Table 2.1.

2.2.2 2D vs 3D Approaches

The decision to use a 2D approach as opposed to a 3D approach is largely application dependent. 2D approaches are "effective for applications where precise pose recovery is not needed or possible due to low image resolution", such as tracking pedestrians in a surveillance

Generative Models	Discriminative Models
Gaussian mixture model	Logistic regression
Hidden Markov model	Support vector machine
Naive Bayes	Neural networks
Boltzmann machine	Boosting
Probabilitistic context-free grammar	Linear regression
Latent Dirichlet allocation	Conditional random fields

Table 2.1: Examples of Generative and Discriminative Models

setting. 2D approaches "represent the easiest and best solution for applications with a single human involving constrained movement and a single viewpoint". Examples include recognizing gait lateral to camera, or recognizing vocabulary of distinct hand gestures made facing the camera.

On the other hand, 3D approaches are more appropriate for indoor (i.e. "controlled") environments where one "desires high level of discrimination between various unconstrained and complex movements". 3D provides a more accurate representation of physical space, as well as better prediction and handling of occlusion and collision. Also, 3D approaches are typically used for action recognition because they are able to provide more meaningful features.

2.2.3 Kinematic vs Shape Models

Model-based approaches use a human body model, which should consider the kinematic structure and body dimensions. Additionally, model-based approaches require a function that, given the model parameters, outputs an approximation of how the model appears in the image domain.

Human body models can be divided into two categories: kinematic models and shape or appearance models. Kinematic models describe the body using body part segments that are linked by joints. Joints are described by the number of degrees of freedom (DOF) they possess, which indicates how many directions the joint can move. Increasing the number of DOF increases the model complexity and increases the number of possible poses. One

way to limit the pose space is by applying kinematic constraints, similar to the methodology of Ju et al. in [63]. The advantage of this technique is that the pose space is limited to only physically possible poses; however, assigning these constraints also increases the computational complexity of the model. Another option is instead to limit the possible parameter values during the estimation phase.

Shape models describe the body as rectangular or trapezoid-shaped patches for 2D methods, or as volumetric shapes (e.g., spheres, ellipsoids, cylinders) or surfaces (e.g., mesh of polygons). A major disadvantage of shape models is that they typically rely on an initialization step, in which the observed person must adopt a specific pose. Feature parameters are then estimated using this pose and then used to track the body part in subsequent images.

2.3 Image Features

In computer vision and image processing, features are used to denote a piece of information which is relevant for solving the computational task. Depending on the application, pixel values alone are highly susceptible to variation due to different clothing and lighting conditions. Extracting certain image features instead of using the original image may improve discrimination and reduce the effect of these variations. Additionally, it may be more computationally cost effective to reduce the feature size and base a decision on a small set of features. Feature vectors are designed to be easy to extract, small, and have the ability to provide the information necessary to discriminate between different poses or objects. Features can be categorized into two groups: dense features and sparse features.

2.3.1 Dense vs. Sparse Features

Dense features use complete image information at the cost of memory and computational speed. However, dense features generally have greater discriminative power than sparse features. Commonly used dense features are the silhouette image vector, silhouette distance

transform image vector, histograms of oriented gradient (HOG), and moments. Commonly used sparse features include turning angle, scale-invariant feature transforms (SIFT), and speeded up robust features (SURF).

In order to decrease the computational cost required of dense features, it is common to reduce the feature space. Feature reduction is concerned with keeping only the features that contribute the greatest amount of information necessary to discriminate between different poses. Principal Component Analysis (PCA) is a common method for reducing the number of features. PCA transforms a highly correlated feature space into a reduced set of uncorrelated variables, called principal components. Principal components are ordered such that the first principal component accounts for as much of the variability in the data as possible.

2.3.2 Commonly Used Features

Silhouettes

Silhouettes and contours can be extracted robustly when backgrounds are reasonably static. Silhouettes are also insensitive to variations due to color and texture. However, their performance is limited due to artifacts, such as shadows or noisy background segmentation. Silhouettes also suffer from depth ambiguities and self-occlusion.

Histograms of Oriented Gradients

Histograms of oriented gradients [64, 65] or HOGs are a dense feature that were recently introduced and have proven to be one of the most robust features, enabling pose recovery without having to extract a person's outline. Histograms of oriented gradients obtain a set of basis vectors that correspond to local features on the human body, such as the shoulders and bent elbows. When using these vectors to reconstruct an image with clutter, the edges that correspond to the person are obtained. Okada & Soatto [66] used histograms of oriented gradients to demonstrate the effectiveness of pose-dependent feature selection to both human detection and pose estimation.

Moments

In image processing, an image moment represents a particular weighted average of the image pixels' intensities, or a function of these weighted averages. The use of moments for pattern recognition was first described by Hu [67] in 1962, in which Hu derives a set of seven scale, translation, and rotation invariant normalized central moments. The first order moment is the center of gravity of an intensity image; the second order moment is the width of an image intensity in one direction. However, the traditional Hu's invariant set is not independent nor complete, as shown in the works of Flusser [68] and Suk [69].

Zernike moments, however, give full translation, scale, and rotation invariance to any arbitrary order. Zernike moments are constructed using a set of complex polynomials which form a complete orthogonal basis set defined on the unit disk. Because of the compact nature of moment features, image moments are typically applied in image compression.

Contour Distance and Turning Angle

Contours represent the outline of the silhouette and, because of their relative ease of extraction, are a commonly used feature. In order to extract the contour, a beginning point is chosen on the edge of the silhouette. The chain code algorithm is then implemented to proceed around the silhouette, extracting the distance traveled and the turning angle required to reach the next point in the contour. The procedure continues until the algorithm arrives at the beginning point, or the edge of the image is reached. The distance is continuous and always returns to zero. The turning angle is discontinuous.

Typically, the distance function maxima represent appendages, as they are the points furthest from the object of interest. A major disadvantage of using the contour feature vector is the assumption that the silhouette is continuous and represents the entire body. In other words, if an appendage is disjointed from the main silhouette, either through occlusion or bad segmentation, that object will not be included.

Scale-Invariant Feature Transform (SIFT)

The motivation behind SIFT is to be able to describe an image object by finding interesting points on the object, which can then be used to recognize that object, regardless of changes in image scale, noise, and illumination.[2]. Typically, such points lie on high-contrast regions of the image, such as object edges. An important characteristic of these extracted features is that their positions relative to one another remain unchanged within a video sequence. However, the relative positions of these features would not remain unchanged in the case of articulated or flexible objects if such objects' geometry were to change between two images in a sequence.

SIFT applies a difference of Gaussians function to a series of smoothed images, then finds interesting points based on where maxima and minima values occur in the computed image. Points and edges with poor contrast are discarded. The interesting points are then described by their dominant orientations (i.e., using HOG). In order to make the algorithm more robust to local affine distortion, the pixel area around the interesting points are considered.

Speeded Up Robust Features (SURF)

SURF[3] is a robust local feature detector partly inspired by the SIFT descriptor. SURF is computationally more efficient than SIFT and may be more robust against certain image transformations compared to SIFT.

While SIFT computes the difference of Gaussians over an image sequence, SURF computes the integral image which can be computed extremely quickly. For features, it computes the sum of the 2D Haar wavelet responses around the interest point.

[2]An application of the SIFT algorithm is patented in the US [70].
[3]An application of the SURF algorithm is patented in the US [71].

2.4 Discussion

This literature review has provided several design options for the proposed system. Low-level design considerations include whether the proposed system will use a generative or discriminative approach; 2D or 3D approach; or use kinetic or shape body models. High-level design considerations provide information for decisions about which image feature(s) to use in order to describe the acquired images.

Because of their robustness in dealing with self-occlusion, the generative approach is likely more appropriate for this application. Additionally, because a generative approach models the whole body configuration, this approach provides the added benefit that regions of interest and statistical information can be directly extracted from the optimized body configuration.

The acquired pressure images will have low image resolution and can be considered as a monocular camera problem. Because of these properties of the acquired pressure images, a 2D approach provides an adequate level of accuracy without much of the complexity associated with 3D approaches. Therefore, a 2D approach is likely more appropriate for the proposed system.

Patients may have limited mobility and may not be able to move into an initialization pose. Shape models typically rely on this initialization step and are therefore not appropriate for this application. Therefore, the proposed system will use a kinematic body model to divide the body into body part segments linked by joints.

Finally, dense features are used to describe the acquired pressure images because of their better discriminative power. Because the pressure images have low image resolution, increased memory costs are anticipated to be small. Additionally, because general hospital practices attempt to distribute pressure as evenly as possible over the body surface, acquired pressure images may not have enough strong characteristic features (edges and corners) needed for sparse feature approaches to be effective.

Chapter 3

Data Acquisition

3.1 Hardware

Data were collected at the patient bedside; study protocols were approved by the Virginia Commonwealth University IRB. Upon enrollment, XSensor, Inclinometer, and Actigraphy data collection began. XSensor and inclinometer were collected for three consecutive days; actigraphy was collected for seven days (Table 3.1).

Data	f_s	Day 1	Day 2	Day 3	Day 4	Day 5	Day 6	Day 7
XSensor	2 Hz	X	X	X				
Inclinometer	2 Hz	X	X	X				
Actigraphy	1 Hz	X	X	X	X	X	X	X

Table 3.1: Data collection schedule. XSensor and inclinometer data were collected continuously for the first 3 days at a sampling frequency of 2 Hz. Actigraphy data were collected continuously for 7 days at a sampling frequency of 1 Hz.

3.1.1 XSensor Pressure Imaging System

The pressure sensing system (XSENSOR Technology Corporation: Calgary, Alberta, CANADA) consists of a 48x144 sensing array of capacitive sensors. Each sensor has a spatial resolution of 0.5 in, for a total sensing area of 24 in x 72 in. The system is calibrated to a pressure

range of 10–200 mmHg and has an accuracy of ±10% full scale. The system operates at an ambient temperature of 10–40°C (50–104°F) and ambient humidity of 5%–90% relative humidity[72, 73]. Pressure data were collected with a sampling frequency of 2 Hz, with each frame consisting of 48 x 144 pixels. Data were stored continuously on a Dell laptop located in the patient's room using XSENSOR's proprietary software program. Associated data files had a .xsn extension.

3.1.2 Inclinometer

Patient backrest elevation was continously monitored using a custom-built device called an inclinometer. The inclinometer hardware consists of three MEMS-based accelerometers (Analog Devices, Model ADXL203, Norwood, MA) and a data acquisition device (NI USB-6009, National Instruments, Austin, TX). The three accelerometers were attached to each of the three steel pivoting sections of the hospital bed, located at the backrest, hip, and knee. A custom LabView Virtual Instrument (VI) was developed in order to apply correct gain and offset parameters to the analog input voltage in order to determine the associated angle. Backrest elevation data were collected with a sampling frequency of 2 Hz, with each sample consisting of three angles for the elevation of the head of bed, hips, and knee flexion. Data were stored continuously on the same Dell laptop used to collect XSensor data in .txt files, each file containing two hours of stored backrest elevation data.

3.1.3 Actigraphy

Patient movement was continously monitored using actigraphy motion loggers (Ambulatory Monitoring Inc., Ardsley, NY). Motion loggers were worn on the patient's non-dominant wrist and ankle, as described in [74]. Motion loggers consist of a piezoelectric ceramic cantilever beam, which generates a voltage proportional to movement. Actigraphy data were collected in Proportional Integrating Measure (PIM) mode, which is a measure of the area under the conditioned transducer signal. PIM mode, therefore, not only measures the frequency and

duration of motion, but also provides a numerical value to represent activity level or rigor of motion. Actigraphy data were collected with a sampling frequency of 1 Hz. Data were stored locally on the motion logger and downloaded to a Dell laptop once the study session was complete. Data were stored in AMI's proprietary software program. Associated data files had a .ami extension.

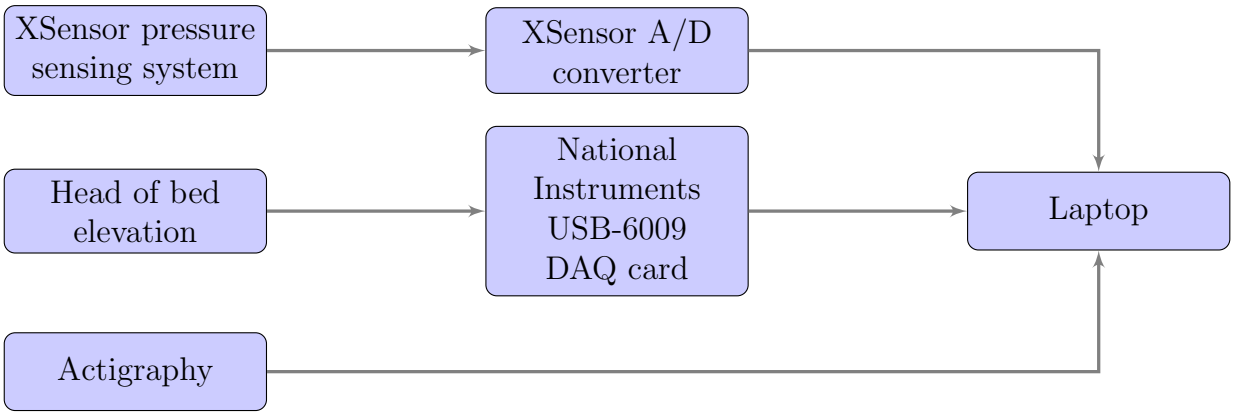

Figure 3.1: Data Acquisition Flow Diagram

3.2 Software

3.2.1 Data Synchronization

Acquired pressure images were processed using MATLAB R2011b on a destop with Intel(R) Core(TM) i7 CPU running a Windows 64-bit Operating System. XSensor (.xsn) files and actigraphy (.ami) files were exported to .txt files using their respective proprietary software. Arm and wrist actigraphy and backrest elevation data were synchronized with XSensor frames using a linear interpolation (Figure 3.2).

3.2.2 Pressure Image Preprocessing

The raw pressure images obtained from the XSensor pressure sensing system were subject to several artifacts as a result of type of sensors used and the clinical environment. The most

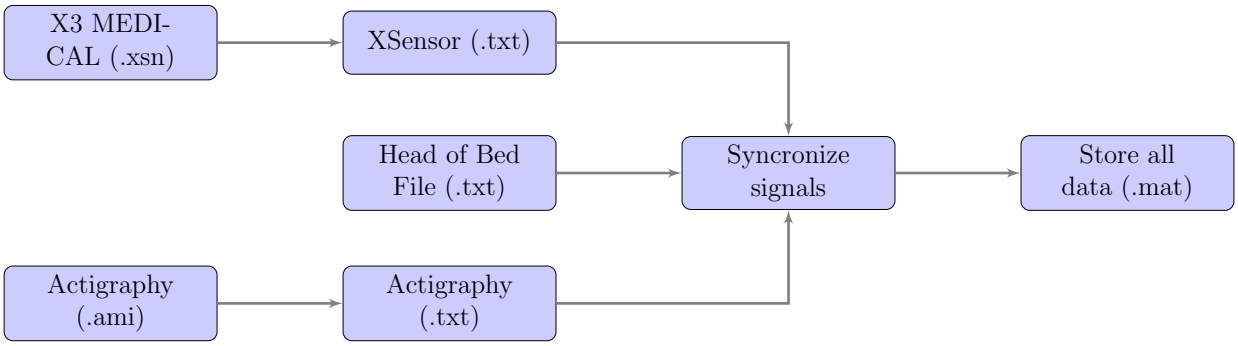

Figure 3.2: Signal Processing Flow Diagram

common artifacts were the presence of spurious artifacts and saturated sensor areas following interaction of the pressure sensing system and a radiology screen. Figure 3.3 shows how an X-ray screen causes one sensor to reach a saturation point. This saturation point remains as a high-value point, even after the removal of the X-ray screen.

Spurious artifacts were removed using the MATLAB built-in function bwareaopen, which removes all connected components that have fewer than p pixels from the binary image. A threshold value of 4 pixels ($\approx$1 in^2) was found to be ideal for deleting small artifacts without potentially deleting important objects, such as the patient's heels.

Because of its insensitivity to extreme values, a median filter was found to be the best method of removing saturated sensor areas. However, because a median filter tends to blur the image and might reduce the magnitude of valid peak pressures, the median filter was applied selectively to areas of very high gradient. In other words, if the magnitude of the image changed rapidly in one particular area, a median filter was applied. This was determined by finding which pixels had a gradient magnitude greater than $\frac{\sigma \cdot \nabla I}{n}$, where σ is a user-determined factor, ∇I is the gradient magnitude, and n is the number of non-zero gradient pixels. For the pressure images collected a σ of 5 was used. The procedure was found to handle saturated sensor areas while preserving true peak pressures better than an adaptive filter, such as a Wiener filter.

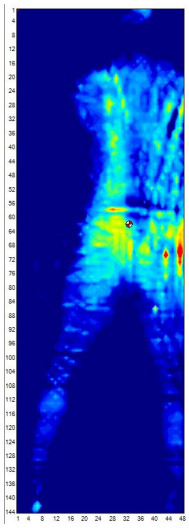

(a) before X-ray

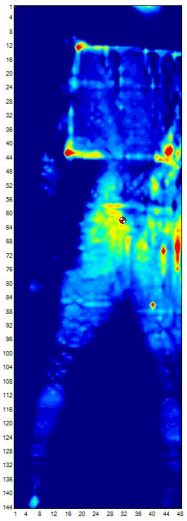

(b) during X-ray

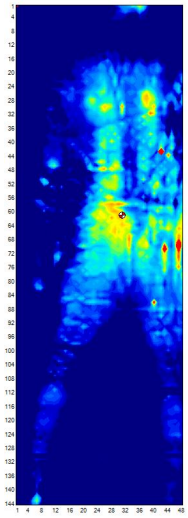

(c) after X-ray

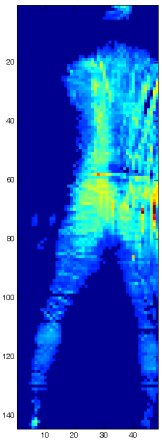

(d) before X-ray, filtered

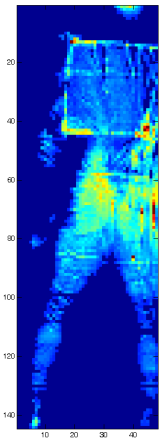

(e) during X-ray, filtered

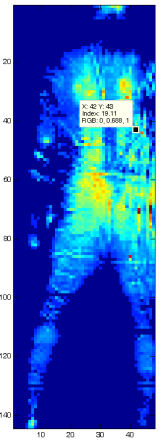

(f) after X-ray, filtered

Figure 3.3: Artifacts are removed using selective median filter

Chapter 4

Pose Classification Algorithm

4.1 Introduction

Marker-less pose classification is a common area of research in the field of computer vision. However, its application to clinical settings and patient monitoring has only recently been studied. Previous methods for monitoring patient position required markers, or worn sensors. The earliest work is presented by Harada et al. [75, 76, 77], in which a motion tracking system based on the physical forces exerted on the mattress surface is described. Yousefi et al. [78, 79] used a Force Sensing Array to classify five different patient poses: supine, left Yearner, right Yearner, left Foetus, and right Foetus. Ostadabbas et al. [80, 81] extended the work of her colleague to create a resource-efficient planning algorithm designed to provide nurses with a more effective turning schedule. Grimm et al. [82, 83] created a pose classification system to improve workflow during a diagnostic tomographic imaging session.

This chapter compares the performance of two classification techniques in order to categorize a patient's pose as left lateral, supine, or right lateral. The classification models included in this comparison were: a multi-layer perceptron (MLP) neural network and a classification and regression tree (CART). The predictor variables considered were: the number of activated sensors on the left side of the image, the number of activated sensors on the right side

of the image, the center of pressure row, the center of pressure column, peak pressure value, contact area, peak pressure row, and peak pressure column. Because it is unclear which features may be important in the classification model, feature selection was implemented using a stepwise regression analysis. Performance of classification techniques were compared using sensitivity, specificity, positive predictive ratio, and negative predictive ratio.

4.2 Materials and Methods

4.2.1 Data

Pressure images were acquired using the XSensor Pressure Imaging System described in Section 3.1.1. The images included in the dataset are a subset from the Skin Integrity and Backrest Elevation (SIBRE) Study conducted at the Virginia Commonwealth University(NIH R01 NR010381-01; M.J. Grap, PI). Patients included in the study were mechanically ventilated recruited from the hospital's Medical Respiratory intensive care center (ICU), Surgical Trauma ICU, and Neuroscience ICU. Patients were at various levels of sedation and generally required nursing intervention in order to re-position. Ten patients were randomly selected and a two-minute session, during which the patient was turned, was extracted from each patient. Thus, each patient has data representative of at least two poses.

Analysis was performed in 2397 images (398 left lateral, 1479 supine, 520 right lateral). Acquired images have a resolution of 48x144 pixels, with each pixel having a spacial resolution of 1.27 cm (0.5 in) for a total sensing area of 60.96 cm x 182.88 cm (24 in x 72 in). Patient pose was determined by visual inspection of the images. Several transition images (e.g., during a transition from left lateral to supine) were included in the dataset and a classification was forced. Figure 4.1 shows the pose classifications of ten patients, as determined by expert visual inspection.

Before building models, the data set was randomly split into training, testing, and validation sets. For the neural network, 60% ($n = 1438$) of the data were reserved for the

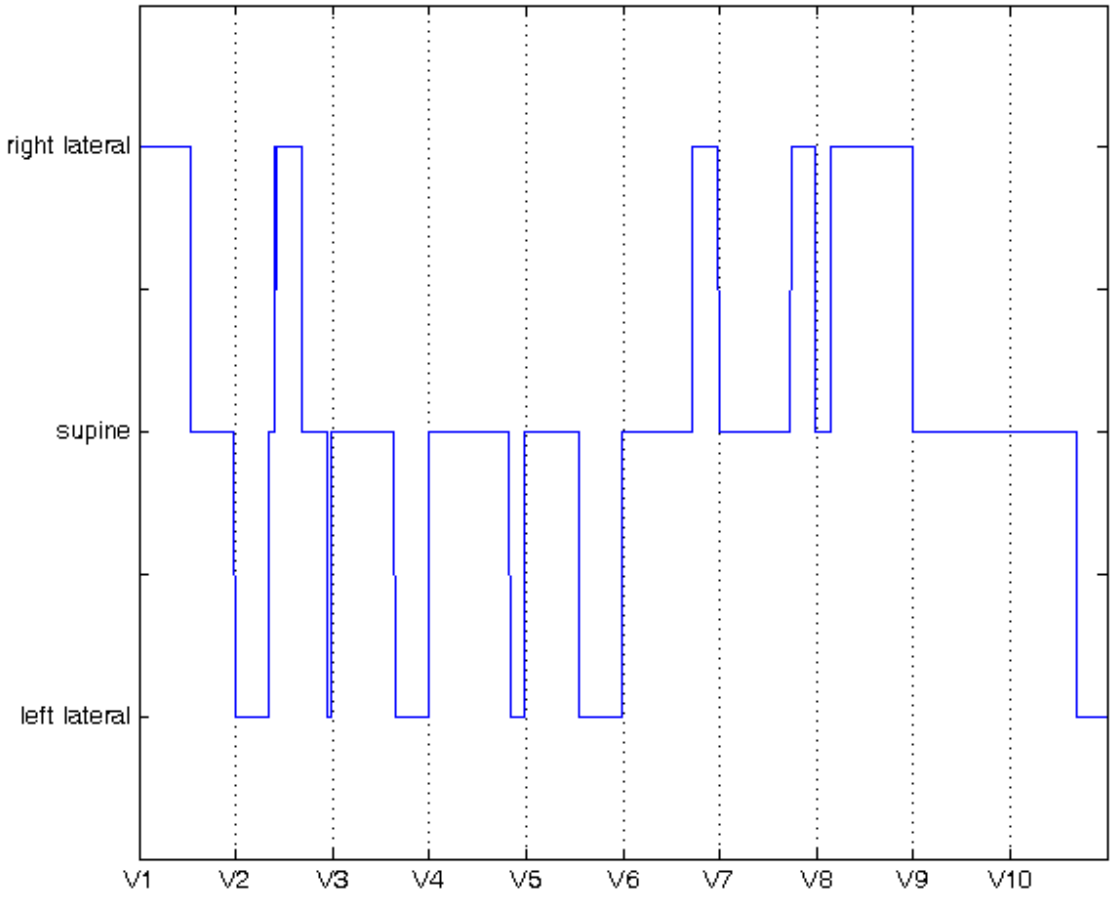

Figure 4.1: Pose classifications of ten patients. The vertical dotted line separates the ten datasets of each of the ten patients (labeled with a "V" followed by an id).

training set, 20% ($n = 479$) for test set, and 20% for validation set. Data were partitioned in such a way as to preserve the classification ratios of the dataset (i.e., so as not to generate a training set with only supine images). The classification tree was cross-validated using a 10-fold partition. MATLAB was used to design the models and compare model performance.

4.2.2 Potential Features

Potential features included the number of activated sensors on the left half of the image, the number of activated sensors on the right half of the image, the x- and y-coordinates of the

center of pressure (COP), the peak pressure, the x- and y-coordinates of the peak pressure, and the total area of activated sensors. The total area and COP data were obtained directly from XSensor software. The other features were obtained using MATLAB software.

4.2.3 Feature Selection

Feature selection reduces the number of features used for model construction by excluding the redundant or irrelevant features. Feature selection is preferable to feature extraction or transformation techniques (i.e., PCA, ICA) because the goal of this step is to understand which features are meaningful. Here, sequential feature selection was applied to iteratively add features to the model until there is no improvement in prediction. The selection process was validated with 10-fold cross-validation without stratification.

4.2.4 Classification Techniques

Multi-Layer Perceptron Neural Network (MLP)

MLP is a feedforward neural network that is trained to classify inputs according to target classes using a back-propagation algorithm. The MLP consists of an input layer, a hidden layer(s), and an output layer. The input layer consists of the features used to describe the training set and the output layer consists of vectors of all zero values except for a 1 in element i, where i indicates which target class the sample represents. This report uses a MLP with one hidden layer composed of 10 neurons (Figure 4.2).

Here, the Levenberg-Marquardt algorithm is chosen as the back-propagation training method because of its speed. The application of Levenberg-Marquardt to neural network training is described in [84]. The Levenberg-Marquardt algorithm uses an approximation of the Hessian matrix[1]

$$H = J^T J \tag{4.1}$$

[1]The Hessian matrix is the square matrix of second-order partial derivatives of a function. The second derivative test uses the Hessian matrix to find extrema of a function.

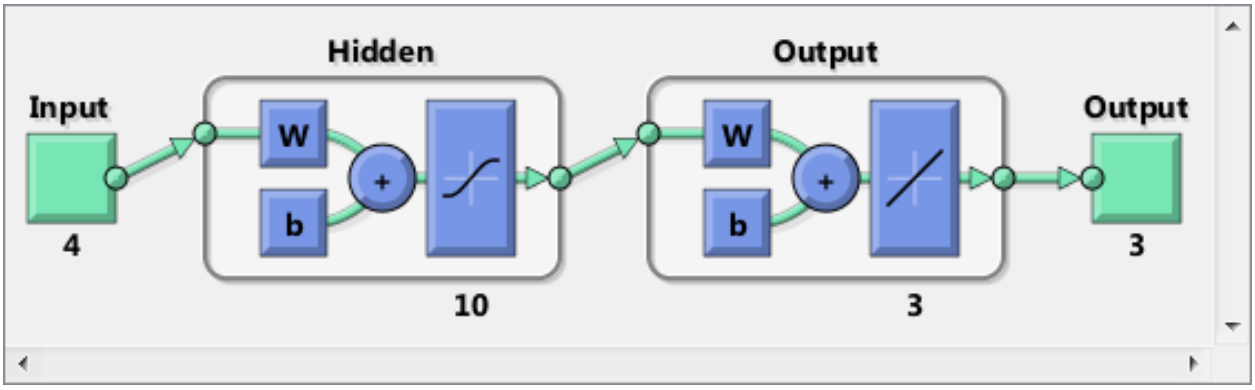

Figure 4.2: The neural network is composed of an input layer, one hidden layer of 10 neurons, and an output layer.

and the gradient is represented by

$$g = J^T e \tag{4.2}$$

where J is the Jacobian matrix that contains first derivatives of the network errors with respect to the weights and biases, and e is the network error vector.

The Levenberg-Marquardt algorithm uses the approximation to the Hessian matrix to update network weights in a Newton-like manner:

$$x_{k+1} = x_k - (J^T J + \mu I)^{-1} J^T e \tag{4.3}$$

where μ is a scalar that acts as a damping factor such that adjustments to the weight vector x are decreased as the equation converges to a solution. When $\mu = 0$, equation 4.3 becomes Newton's method, using the approximate Hessian matrix found by equation 4.1. Conversely, when μ is large, equation 4.3 becomes gradient descent with a small step size. Because Newton's method is faster and more accurate near an error minimum, μ is decreased after each successful step so that the Levenberg-Marquardt algorithm behaves similar to Newton's method as it approaches convergence.

Classification and Regression Tree (CART)

CART is a non-parametric decision tree learning technique that can be used for regression or classification, depending on whether the dependent variable is numerical or categorical, respectively. MATLAB trees are binary; in other words, each step in a prediction involves checking whether the value of a single predictor variable is less than or greater than a particular threshold value. The basic procedure for creating a decision tree is:

1. Start with all input data and examine all possible binary splits on every predictor.
2. Select a split with the best optimization criterion.
3. Impose the split.
4. Repeat recursively for the two child nodes.
5. Stop splitting when any of the following hold:
   (a) The node is pure, meaning that the node contains only observations of one class.
   (b) There are fewer than a minimum number of observations in the node.
   (c) Any split imposed on this node would produce children with fewer than MinLeaf observations.

For a regression problem, mean-squared error is a common optimization criterion. For a classification problem, such as this, commonly used optimization criteria include the Gini's diversity index, twoing, and deviance. For this study, the Gini diversity index was used. The Gini diversity index of a node is

$$g(t) = 1 - \sum_i p^2(i|t), \tag{4.4}$$

where the sum is over the classes i at the node, and $p(i|t)$ is the observed fraction of classes with class i that reach the node t. The Gini index is a measure of node impurity: a node

with just one class (a *pure* node) has Gini index 0. Conversely, when the observations in a node are evenly distributed across all categories, the Gini index takes its maximum value of $1 - (1/k)$, where k is the number of categories.

The Gini criterion function for split s at node t is defined as

$$\Phi(s,t) = g(t) - p_L g(t_L) - p_R g(t_R) \tag{4.5}$$

where p_L is the proportion of cases in t sent to the left child node and p_R is the proportion sent to the right child node. Therefore, the split s that maximizes the value of $\Phi(s,t)$ is chosen in order to optimize the tree classification.

The CART can also be pruned for simplicity. Here, the tree was pruned using the test sample in order to determine the best pruning level. Figure 4.3 illustrates the pruned CART.

4.3 Results

A comparison of the sensitivity (SEN), specificity(SPE), positive predictive rate (PPR), and negative predictive rate (NPR) are presented in Table 4.1. Both MLP and CART performed well with classification accuracy approximately 99% for all three pose classifications.

Closer inspection of the incorrect classifications revealed that disagreements occurred when evaluating a transition image, where pose may be ambiguous. The confusion matrices produced by the two clasification methods (Figure 4.4) reveal that, while both algorithms generally have good accuracy, CART is somewhat better at correctly classifying the transition images.

The pose classification algorithm performs better than other classification methods. Hsia et al. [85] achieved 81.4% average classification accuracy differentiating between six different sleeping postures (right and left Yearner, right and left Foetus, log, and supine) Yousefi et al. [78] report an overall accuracy of 97.7%.

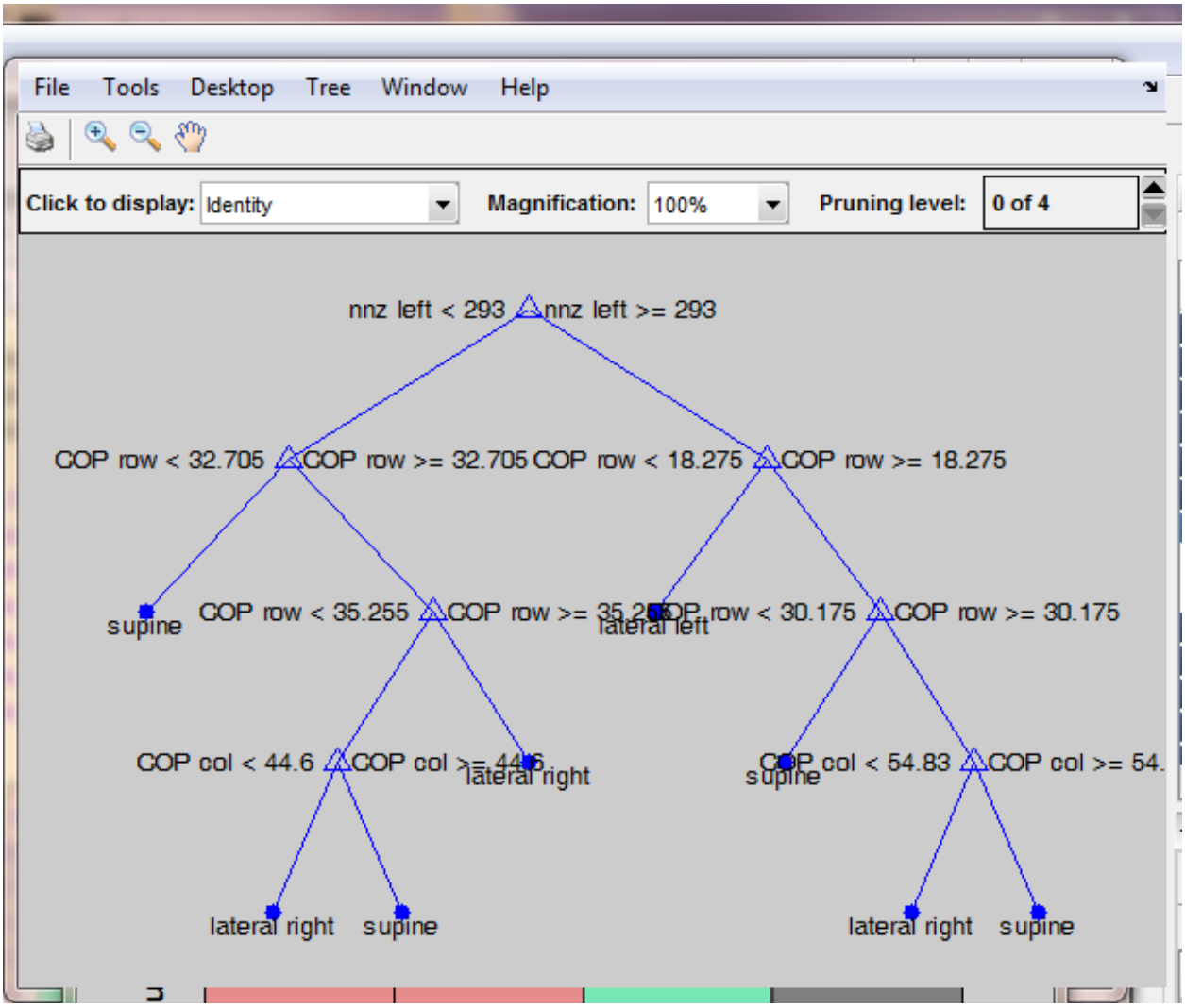

Figure 4.3: The pose classification tree separates images based on the number of activated sensors on left and right halves of image (nnz left and nnz right, respectively), as well as the COP row and COP column.

4.4 Discussion

Repositioning is generally regarded as one of the most important and effective measures for preventing pressure ulcers. The classification algorithm presented here provides an efficient and accurate way of monitoring re-positioning. The algorithm performs with an overall accuracy of 99.5%, which is better than the results of several other studies.

Additionally, this study uses pressure images acquired from patients in a hospital setting. This demonstrates that the classification method is, in fact, robust enough to handle artifacts

Pose	Model	SEN	SPE	PPR	NPR
Left Lateral	NN	99.50	99.90	99.50	99.90
Left Lateral	CART	99.50	99.95	99.75	99.90
Supine	NN	99.73	99.24	99.53	99.56
Supine	CART	99.86	99.35	99.60	99.78
Right Lateral	NN	98.85	99.89	99.61	99.68
Right Lateral	CART	99.23	99.95	99.81	99.79

Table 4.1: Comparison of the performance of the models

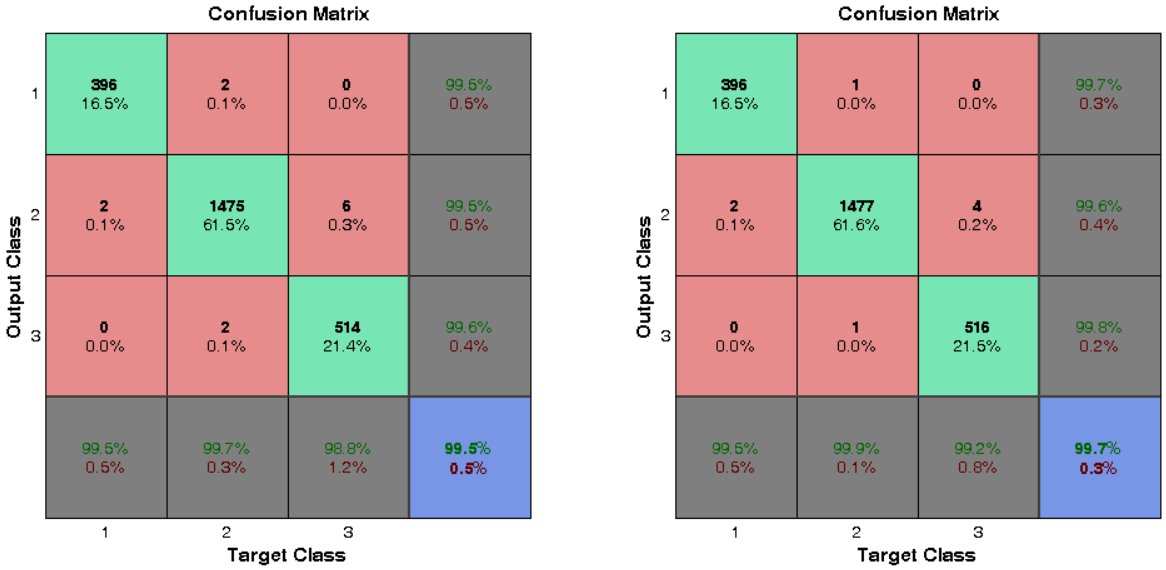

(a) MLP Neural Network

(b) CART

Figure 4.4: Results of MLP Neural Network and CART are compared using their confusion matrices.

due to manual turning, such as hospital staff leaning on the bed to re-position the patient, or instances where the patient is partially off the sensing area.

This method can be used for patient monitoring and, ultimately, for aiding clinical decision-making with regard to effective turning schedule and pressure redistribution. Additionally, the developed pose classification algorithm is utilized in segmenting the patient's body into at-risk regions of interest, as described in the following chapter.

Chapter 5

Segmentation Algorithm

5.1 Introduction

Recently, human motion analysis has seen a rapid advancement. However, human motion analysis is typically applied to optical sensors. Only recently have alternate image and video modalities, such as range and pressure sensors, been considered. Human motion analysis holds great promise in the field of pressure ulcer research.

Studying the mechanical loading intensity and duration of specific anatomical sites may greatly enhance our understanding of pressure ulcer development. This would involve continuous pressure monitoring in a clinical setting and data analysis would require *post hoc* analysis of a large amount of data. In order to decrease the time demands of such analysis, a human motion analysis system is proposed in order to automatically segment pressure images into specific anatomical sites deemed high-risk for developing pressure ulcers.

There have only been a few attempts at such a system. Sakai et al. [54] developed a thermoelastic polymer mattress in order to record whole-body interface pressure for up to 48 hours in a clinical setting. The collected pressure images were segmented into three parts: head-dorsal, buttocks, and lower limb regions (Figure 5.1a). The head-dorsal and buttocks regions were separated by the waist, which was defined at the slimmest point in

the image. The buttocks and lower limb regions were separated by the base of the thigh, which was considered as the first column in which no sensing points were activated below the waist. While simple, this segmentation algorithm fails to describe the variety of images produced by the pressure sensing system used in this research project. It assumes that the patient is in a supine pose, that the head-dorsal and buttocks region are a single connected component separate from the heels, and that the patient's waist remains in a fairly vertical plane. Moreover, the system does not account for occlusion due to clinical interventions.

Grimm et al. [82] developed a segmentation procedure in order to improve clinical workflow during a diagnostic tomographic imaging session (Figure 5.1b). Both range imaging and pressure imaging sensors were considered in order to estimate patient pose. The algorithm used an articulated 3D body model rendered using OpenGL. The model pose parameters were optimized using a genetic algorithm. Anatomical landmarks were chosen based on how easily they can be differentiated, not necessarily on their clinical relevance to pressure ulcer research.

The proposed project describes a markerless motion analysis system that can eliminate the manual analysis required in order to segment pressure images into high-risk regions. Information provided by such a system can greatly improve the ability of researchers and clinicians to understand how pressure ulcers develop in a hospital environment. As a consequence, the system could also guide decisions in clinical interventions.

5.2 The Model

The 2D articulated model of the human body used to generate a hypothesis silhouette was composed of connected ellipses(Figure 5.2). The model configuration is described by the vector $\theta \in \mathbb{R}^{23}$, in which θ is decribed by the tuple (x, y, B) where $x \in \mathbb{R}^8$ and $y \in \mathbb{R}^8$ describe the 8 points used to define the connected major axes of the 7 ellipses and $B \in \mathbb{R}^7$ describes the minor axes half-lengths of the ellipses.

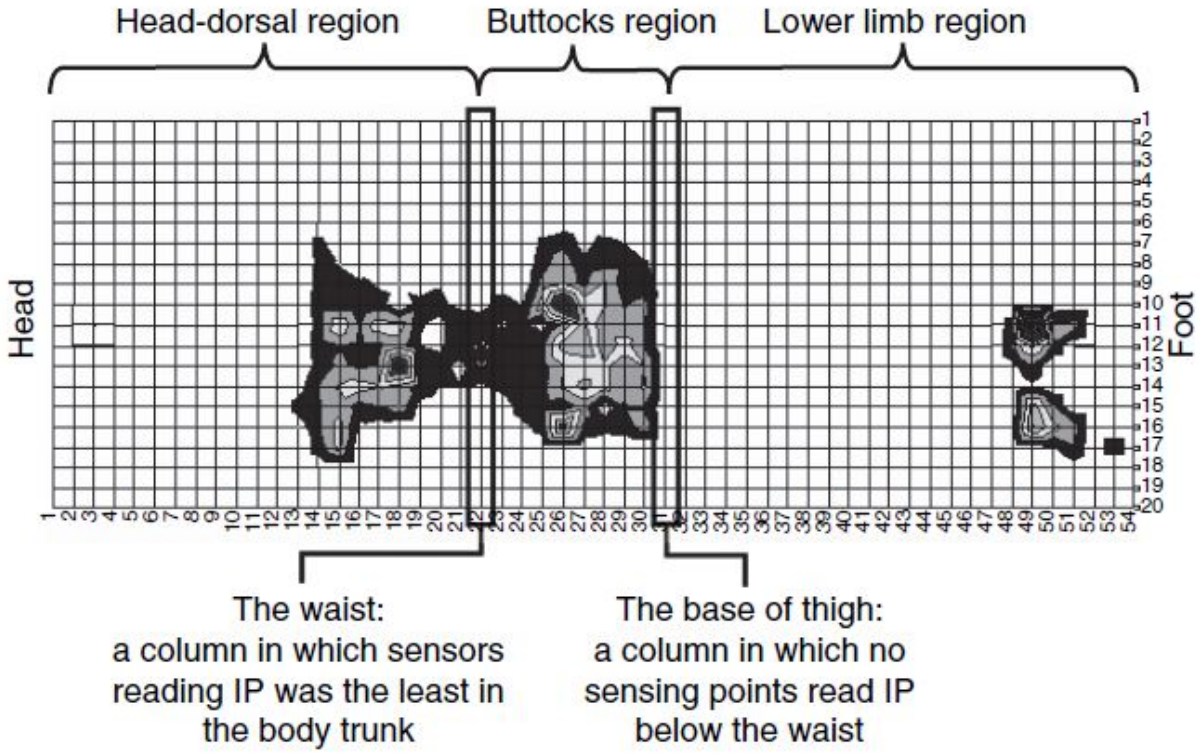

(a) Sakai (2009)

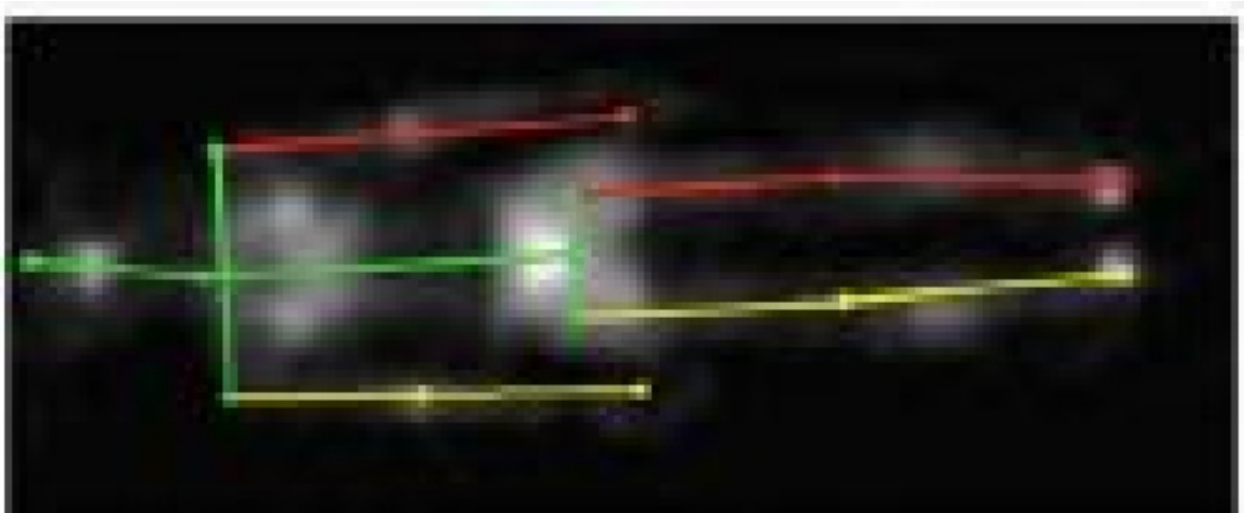

(b) Grimm (2012)

Figure 5.1: Sakai et al. [54] assumed a specific patient pose for segmentation (a). In contrast, Grimm et al. [82] developed a robust segmentation algorithm using a kinematic model.

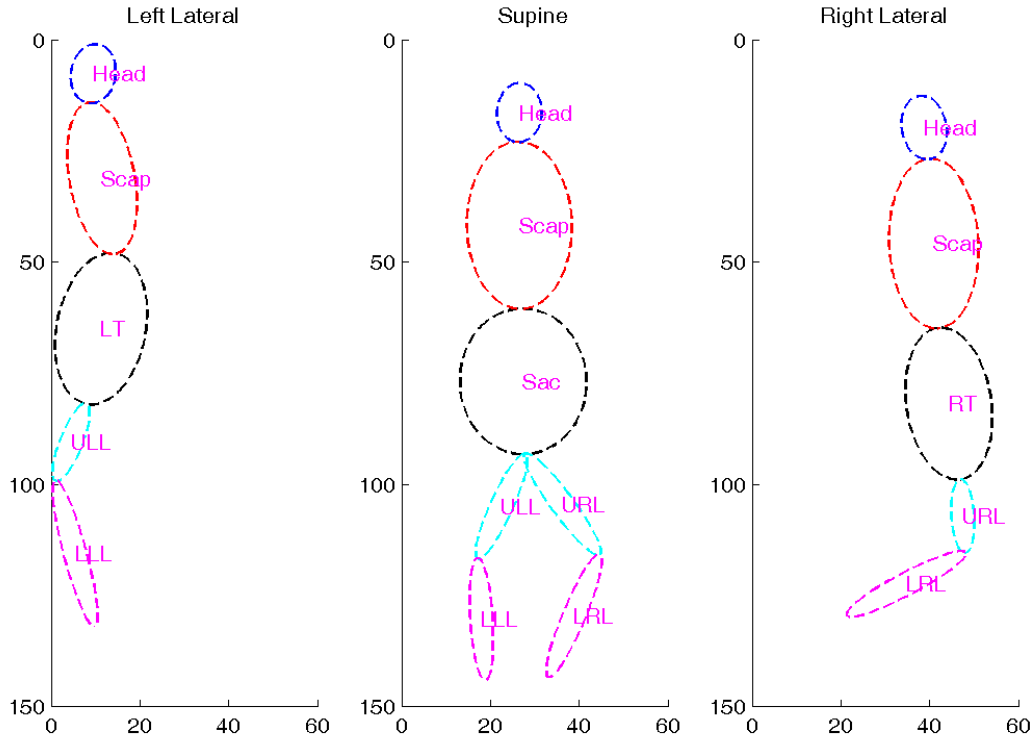

Figure 5.2: 2D articulated body model

Because the 2D patient pose and articulation in the coronal plane (e.g., the plane parallel to the hospital bed) holds sufficient information, the articulation of the model is restricted to movement in this plane. This reduces the dimensionality of the pose search space.

As described in Harada [75], a full body model was not able to handle the lower arm and hand positions well because these body parts generally do not appear in measured pressure distribution images. Therefore, these body segments were simply excluded from the model. The articulated model for all three poses is depicted in Figure 5.2.

5.3 Preprocessing

Pressure images were preprocessed using the procedure described in section 3.2.2. However, silhouettes still proved noisy, with jagged boundaries, spurious pixels, or missing inner pixels.

5.4 Pose Optimization

Pose classification was determined using the CART algorithm described in Chapter 4. Following this step, pose optimization was achieved in a two-part procedure. First, an approximation of the input parameters θ were obtained by sampling several pose configurations and determining which configuration best minimized the cost function (as described in section 5.4.4). The approximated parameters θ_i were further refined using the Nelder-Mead simplex method in order to minimize the cost function. Such that the final parameters $\hat{\theta}$ satisfied

$$\hat{\theta} = \underset{\theta}{\text{Min}}\, f(I|\theta) \tag{5.1}$$

where the cost function $f(I|\theta)$ is explained in Section 5.4.4.

5.4.1 Finding Extremities

In order to initialize a framework for potential skeleton models, the algorithm first searched for the extremities (head and feet) within the image. Extremities were considered as the points furthest from the center of pressure. The center of pressure was calculated as:

$$(\mu_x(I), \mu_y(I)) = (\frac{\sum_x r_i p_i}{\sum_{x,y} p_i}, \frac{\sum_y r_i p_i}{\sum_{x,y} p_i}) \tag{5.2}$$

The Chamfer distance was computed for all points within the silhouette. The points with the greatest Chamfer distance were found and an agglomerative hierarchical cluster analysis was performed in order to separate the furthest points into the correct extremity clusters. If the patient was supine, then points were recursively included in the cluster analysis until

three separate clusters were identified. If the patient was in a lateral left or lateral right position, then the algorithm was repeated until two separate clusters were identified.

The cluster corresponding to the patient's head was assumed to be the cluster closest to the top of the image (e.g., the cluster with the least row values). In the case where the patient was supine, the left heel was differentiated from the right heel and assumed to be the cluster closest to the left of the image (e.g., the cluster with the lesser column values).

5.4.2 Sampling Procedure

Once the extremities were found, their values were entered into the pose parameter vector θ. The points between the extremities were determined by sampling potential values that could be found in a clinical context. Potential angles between points were determined using normal range of motion values [86]. The pertinent normal range of motion values used for determining these locations are summarized in Table 5.1. Distances between points and the half-length minor axes values for b were determined based on observed value ranges directly from the acquired pressure images. This was used as opposed to actual patient measurements because the acquired pressure images may not reflect normal values well due to folding of the sensor or changes in backrest elevation.

For this experiment, a total of 100 potential pose parameter vectors were generated for each image. The model was set to each of these vectors and their cost evaluated using the cost function (Equation 5.3). The vector that had the lowest cost was passed to the next step for further optimization.

5.4.3 Cost Function Minimization

The pose optimization algorithm is based on the Nelder-Mead, or downhill simplex, method as described in Lagarias et al. [87]. The Nelder-Mead simplex method is a commonly used direct search method for minimizing an objective function in a many-dimensional search space. The method uses the concept of a simplex, which is a special polytope of $N + 1$

Joint	Motion	Range (°)
Neck (Cervical Spine)	Flexion(tilt head towards chest)	0-45
	Extension(tilt head back)	0-60
	Lateral Extension (tilt head towards shoulders)	-45–45
Hip (Lumbar Spine)	Abduction (leg crosses center-line)	0-45
	Adduction (leg moves away from center-line)	45-0
	Lateral Flexion(tilt towards side)	0-25
	Flexion(forward from waist)	0-125
	Extension(lean backwards from waist)	115-0
Knee	Flexion	0-130

Table 5.1: Normal Values for Range of Motion of Joints used in skeleton model, adapted from [86].

vertices in N dimensions. The method approximates a local optimum of a problem with N variables when the objective function varies smoothly and is unimodal (e.g.,the function has no local maxima). The method achieves this by modifying the simplex repeatedly by reflecting, expanding, contracting outside, contracting inside, or shrinking the simplex (see Appendix B). The iteration of the Nelder-Mead simplex method terminates when the cost function $f(I|\theta)$ has converged to a minimum (i.e., no longer decreases) or when a maximum number of iterations is reached.

5.4.4 Image Cost Function

In order to evaluate how well the hypothesized silhouette fit with the acquired pressure image, a cost function similar to that used by Balan et al. [88] was applied. The cost function provides a measure of similarity between the image silhouette, F^I, and the hypothesized silhouette, F^H.

In order to compare the image silhouettes, if a pixel belongs to the image silhouette (e.g., $p(x, y) \in F^I$) but not the hypothesized silhouette (e.g., $p(x, y) \ni F^H$), the error is computed based on the shortest distance between that pixel and the hypothesized silhouette, and vice versa. In order to compute this distance, a Chamfer distance map is created for the the image silhouette, C^I, and for the hypothesized silhouette, C^H. The generated silhouettes

and Chamfer distance maps are depicted in Figure 5.3.

The final silhouette should minimize the error generated by the hypothesized silhouette exceeding the image silhouette ($F^H \cdot C^I$) as well as the error generated by the hypothesized silhouette failing to completely overlap with the image silhouette ($F^I \cdot C^H$). The cost function $f(I|\theta)$ minimizes both these constraints by applying a weighting term and summing the two errors over all pixels, such that

$$f(I|\theta) = \frac{1}{|p|}\Sigma_p(aF_p^H \cdot C_p^I + (1-a)F_p^I \cdot C_p^H) \tag{5.3}$$

where $a = [0, 1]$ and is intended to weigh the first term more heavily because images silhouettes will generally be wider than the region of interest due to pressure redistribution techniques.

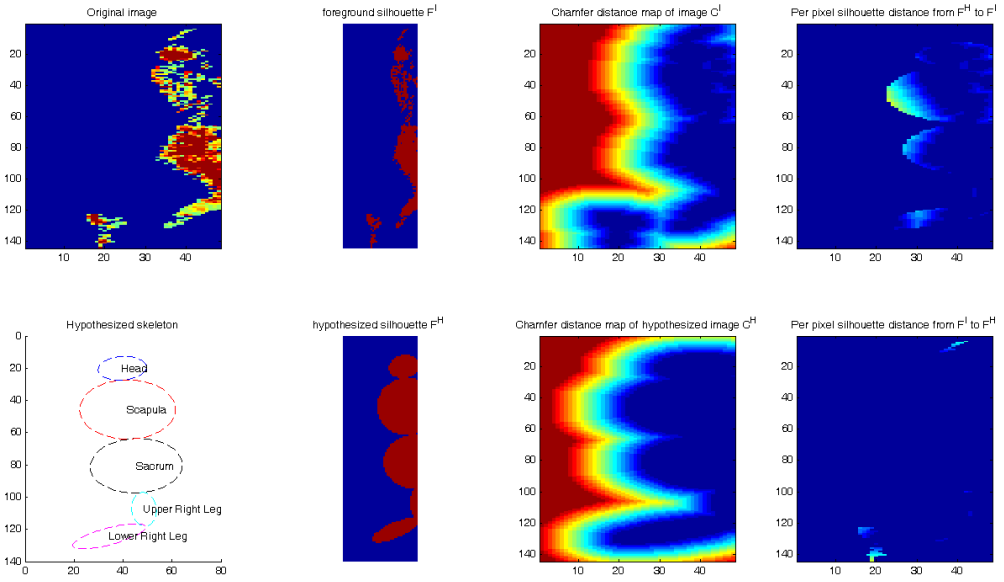

Figure 5.3: The construction of the image cost function is illustrated. The image in the top left illustrates the acquired pressure image. The image in the bottom left illustrates the connected ellipse tree. The hypothesized and foreground silhouettes are shown. Chamfer distance maps hold a value of 0 inside the respective silhouettes. Silhouette distance comparing differences from hypothsized skeleton to true skeleton (top right), and differences from true skeleton from hypothesized skeleton (bottom right).

5.5 Determining Regions of Interest

A label map was created in order to mark the regions of interest on the pressure image.

Sacrum or Trochanter

If the patient was supine, then the pixels enclosed by the third ellipse from the top were marked as sacrum. If the patient was in a lateral position, then the pixels that were enclosed by the third ellipse were marked as right or left trochanter.

Scapula

The scapula was marked only in the supine position. The midline of the scapula coincided with the major axis of the second ellipse from the top. Thus, pixels to the left of the major axis were marked as the left scapula and pixels to the right of the major axis were marked as the right scapula.

Heels

Heels were determined as the connected component nearest to the point marking the heel. In order to ensure a good heel candidate, the connected component had to meet a size range. If the size requirement was not met, then heels were considered to be any pixel within a distance d_h of the heel point. If the patient was in a lateral position, then only one heel was assumed on the pressure sensing area.

5.6 Experimental Results

The automatic segmentation results were compared to the model placements of an expert. A custom-built MATLAB graphic user interface (GUI) was designed to enable the expert to move model markers over acquired pressure images easily (Figure 5.4).

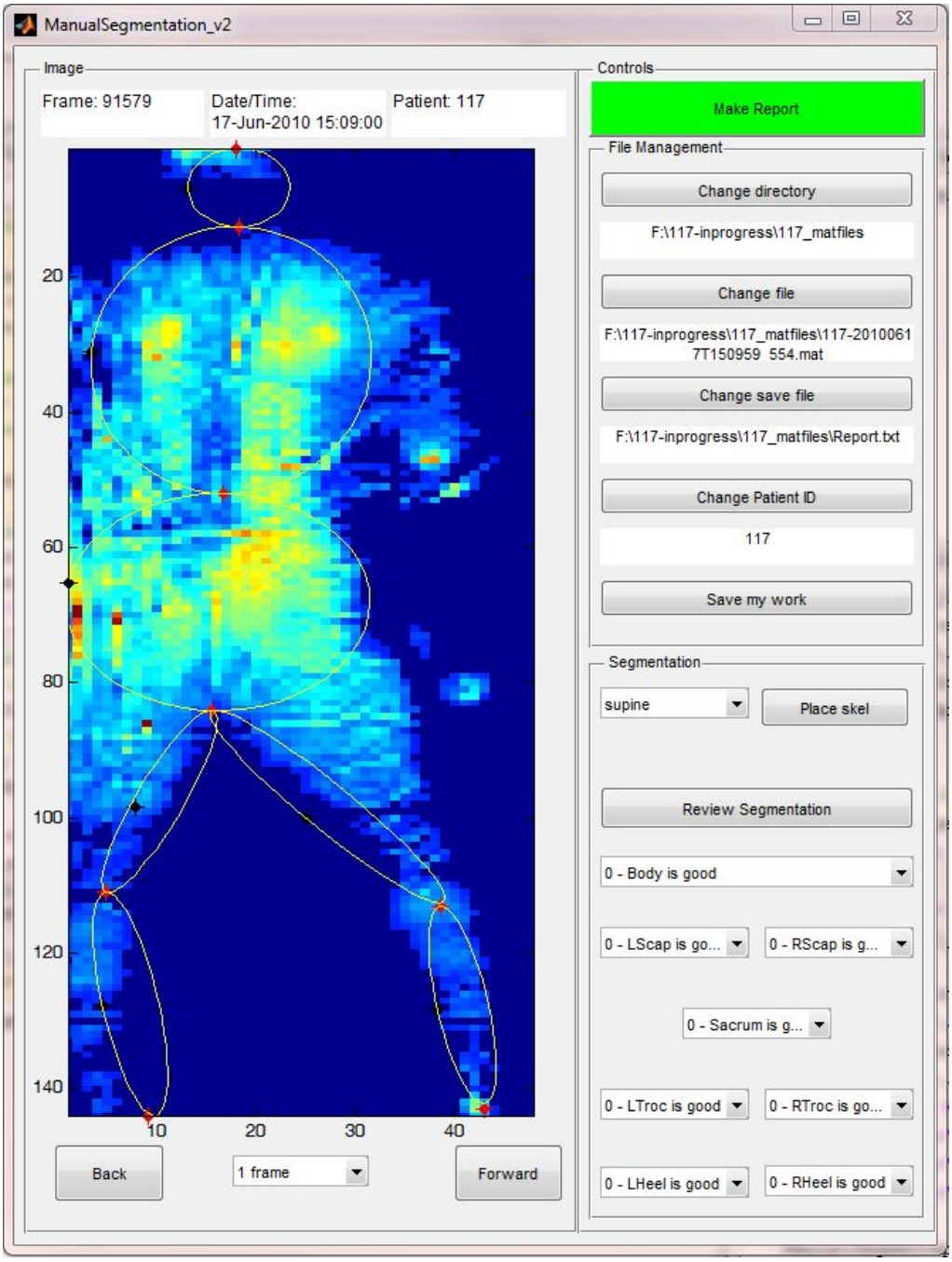

Figure 5.4: An expert manipulated the model over the acquired pressure images using a custom-built segmentation app.

Results were based on how well the automatic segmentation algorithm was able to find the same peak pressure location as the user for each region of interest. If the automatic and manual segmentations disagreed on peak pressure location, then the average distance (in pixels) between the two peak locations were determined. Additionally, the ability of the

automatic segmentation algorithm to accurately classify a pixel in the image as belonging to the region of interest or not was computed using the equation

$$accuracy = \frac{TP + TN}{TP + FP + FN + TN} \tag{5.4}$$

where TP represents the number of pixels correctly classified within the ROI, TN represents the number of pixels correctly classified as being outside the ROI, and the denominator represents the total number of pixels in the image.

However, because an expert is likely to segment a smaller area, it may be more fitting to evaluate the percent overlap, compared to the total area in the ROI marked by the automatic algorithm and by the expert. The equation for area overlap then is

$$overlap_{expert} = \frac{(TP + FP)_{expert} \cup (TP + FP)_{alg}}{(TP + FP)_{expert}} \tag{5.5}$$

$$overlap_{alg} = \frac{(TP + FP)_{alg} \cup (TP + FP)_{expert}}{(TP + FP)_{alg}} \tag{5.6}$$

where the numerator represents the number of pixels that were classified by both the expert and the algorithm as belonging in the ROI, and the denominator represents the total number of pixels that the expert and the algorithm classified as belonging in the ROI, respectively.

Table 5.2 summarizes the accuracy of the segmentation algorithm. Overall, the results show that the algorithm was generally better at finding the sacrum and trochanter.

ROI	**Agreement(%)**	**Error (pix)**	**Accuracy(%)**	**Overlap of Manual(%)**	**Overlap of Auto(%)**
Right Scapula	63.7881	15.7531	97.5935	58.0082	65.3025
Left Scapula	67.6262	14.9238	97.6719	63.0185	64.7535
Right Heel	45.0146	13.8007	99.6508	46.5476	48.1120
Left Heel	51.4393	15.8370	99.7713	46.2912	47.3665
Sacrum	87.4009	15.1943	96.1754	73.0380	76.0113
Right Trochanter	90.6133	24.2657	99.2751	65.4739	62.9130
Left Trochanter	93.6170	14.9430	99.2849	61.3709	57.0138

Table 5.2: Segmentation Results

A closer look at typical errors in placement of landmarks by the automatic segmentation algorithm reveals why heels had the highest error. In the left lateral example shown

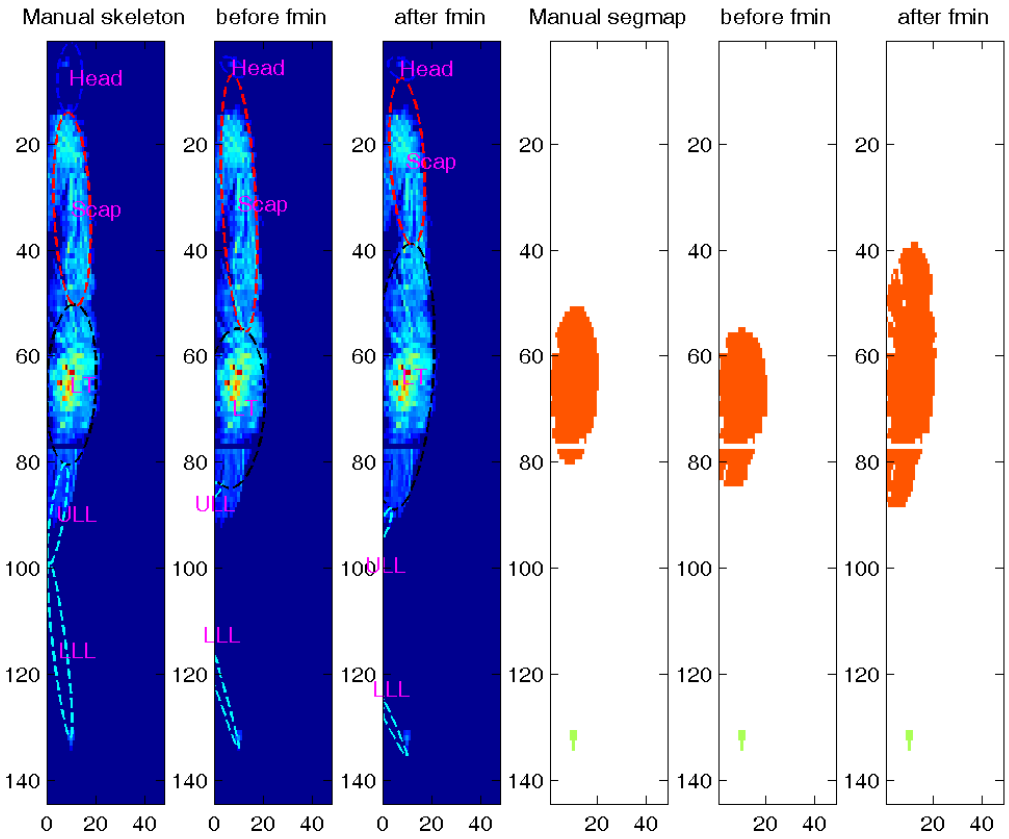

Figure 5.5: A manually segmented pressure image is compared with an automatically segmented pressure image, with the patient in a left lateral position. The sampling procedure generated a valid parameter vector; however, the function minimization procedure deviated from the expert user's configuration. This is because the function minimization attempts to match the silhouette as closely as possible.

in Figure 5.5, the algorithm correctly assumed that the connected component located in the bottom of the image was the patient's right heel. However, in the supine example in Figure 5.6 shows that the patient's left foot was not on the pressure sensing area. While the expert showed this by marking the left heel on an empty region of the image, the algorithm assumes that the heels must exist in the image. Therefore, the algorithm picked the two connected components in the image most likely to be heels.

Additional examples in the supine position (Figures 5.7 and 5.8) are provided. Figure 5.7 shows how well the function minimization algorithm was able to improve the initial guess pro-

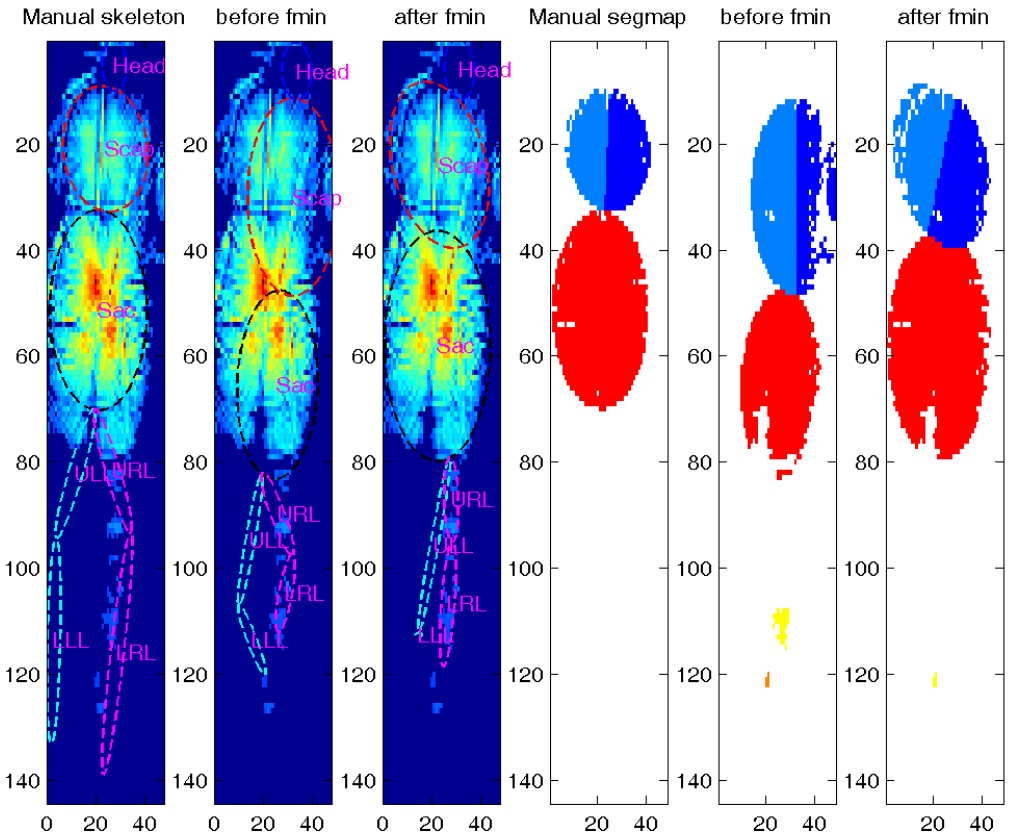

Figure 5.6: A manually segmented pressure image is compared with an automatically segmented pressure image, with the patient in a supine position. Note that the patient's left foot is not on the pressure sensing area and the expert user marks the location of the right foot in an ambiguous area. The algorithm instead assumes that both left and right feet are in the sensing area and marks the patient's right calf as both left and right heel.

vided by the sampling procedure. Figure 5.8 shows how poorly the algorithm approximates the pose parameters when the head is not easily located in the pressure sensing area.

In the right lateral example shown in Figure 5.9, the algorithm placed the right heel at an appropriate location. However, the problem lies in the labeling algorithm following landmark placement. Because the labeling algorithm seeks to label only one connected component in the image as the heel, it picked the connected component closer to the bottom edge (the patient's toes) instead of the connected component that actually represents the heel. This problem with the labeling algorithm is not inherent only in cases where the heel and toes

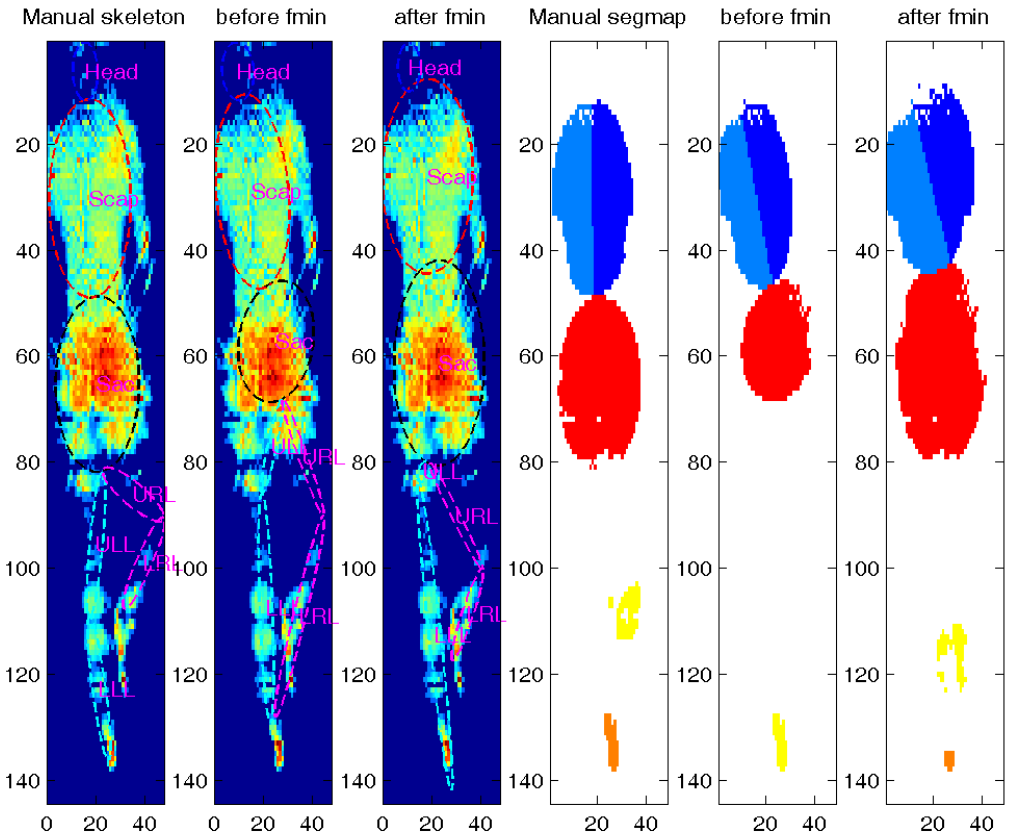

Figure 5.7: A manually segmented pressure image is compared with an automatically segmented pressure image, with the patient in a supine position. Note that the the sampling procedure is unable to mark the right feet accurately. The function minimization procedure, however, is able to address the problem and generates a good approximation of both the left and right feet. Note also that the function minimization procedure improves the fit of the sacrum and the scapula.

are present, but also when there are artifacts due to the pressure sensing equipment, such as in the case of interruptions across a sensing strip.

5.7 Conclusion

Limitations

As stated in section 5.4.1, extrema were assumed to be within the image and located at the points furthest from the image center of pressure. This assumption may lead to poor

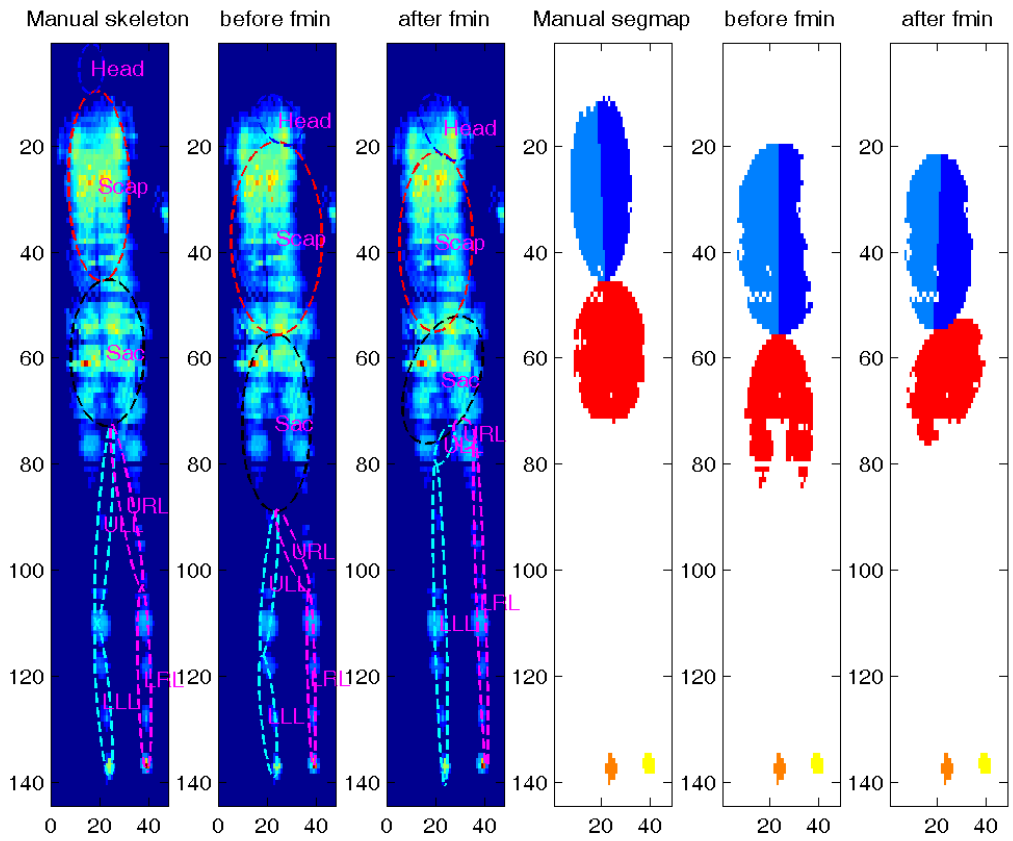

Figure 5.8: A manually segmented pressure image is compared with an automatically segmented pressure image, with the patient in a supine position. Note that the expert user assumed the head was off the pressure sensing area and placed head markers in a region with no pressure. The automatic algorithm, however, assumes that the head is located in the pressure sensing area and attempts to place the skeleton in such a way that this condition is satisfied.

segmentation if the head and feet are not within the sensing area. Additionally, in the case where the knees are bent (e.g., the foot is tucked), then the assumption that the feet are the most distant point will cause poor extrema identification.

The proposed algorithm uses a top-down approach, using the image to propose a whole skeleton structure. A bottom-up approach, in contrast, would extract body segments based on their appearance, and then assemble a skeleton structure. Combining the proposed algorithm with a bottom-up approach may overcome the limitations associated with finding extremities. For example, a bottom-up approach might involve training examples to identify

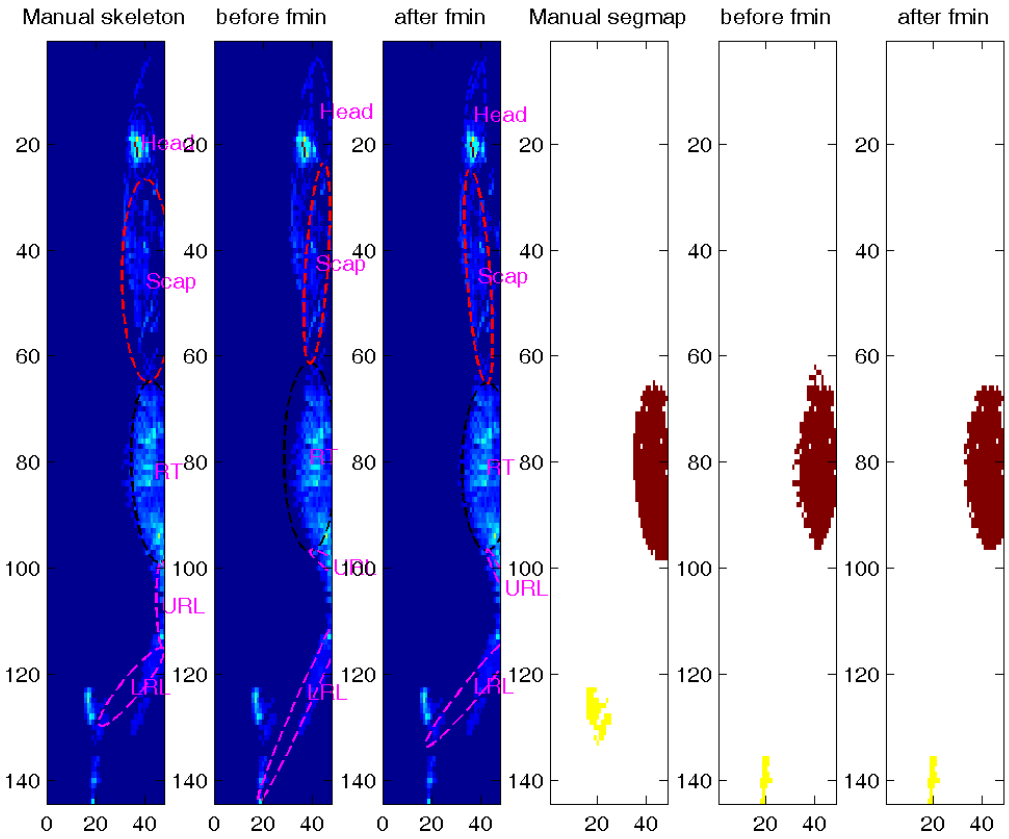

Figure 5.9: A manually segmented pressure image is compared with an automatically segmented pressure image, with the patient in a right lateral position. The sampling procedure assumes the heel to be the lowest component of the image, and therefore incorrectly marks the patient's toes as a heel. The function minimization algorightm is able to more accurately mark the heel because of the added cues from the silhouette of the patient's leg.

body parts with strong features, such as the head and feet. If the identifier is unable to find the head and feet in the image, then the algorithm would use the top-down approach.

The average computation time, with 100 randomly generated samples, was 16.3 seconds per frame. Unfortunately, this process is too computationally expensive to be feasible in a real-time environment. However, the accuracy of the algorithm suggest that this may be an effective way to initialize a skeleton, especially if combined with a bottom-up approach. Predictive techniques (such as Kalman filtering) can then be used in order to perform fast tracking of body segments.

Contribution

The segmentation algorithm presented is a major contribution to pressure ulcer research. With the exception of Sakai et al. [54], the algorithm described here is the only method that has been validated using pressure images acquired in a clinical setting. Similar to Sakai, the presented algorithm is capable of dealing with inconsistencies due to changes in hospital bed surface, i.e., changes in perceived body segment lengths due to changes in bed angles. However, it proves to be more robust than Sakai's algorithm, which must assume that the patient is supine. Additionally, the proposed algorithm is robust enough to handle a variety of poses encountered in a clinical setting.

Preface

The following manuscript is in preparation for publication in a peer-reviewed journal focusing on wound research.

Effects of Behavior State and Backrest Elevation on Skin Interface Pressure

Anathea Abad Pepperl*, Doctoral Candidate

Melissa Bucalan Rooney†, Graduate Research Assistant

Angela Bataille†, Project Director

Ruth Srednicki Burk†, Doctoral Candidate

Christine Schubert, PhD‡, Associate Professor

Paul A. Wetzel, PhD*, Associate Professor

Mary Jo Grap, PhD, RN, FAAN†, Nursing Alumni Distinguished Professor

* Biomedical Engineering Department, School of Engineering, Virginia Commonwealth University, Richmond, VA; † Adult Health and Nursing Systems Department, School of Nursing, Virginia Commonwealth University, Richmond, VA; ‡ Air Force Institute of Technology, Wright-Patterson Air Force Base, Dayton, OH

Chapter 6

Role of Self-Positioning

6.1 Introduction

Immobility has long been identified as a critical risk factor [89, 90, 91, 92, 93]; however, only a few studies have shown how independent self-positioning might mitigate the risk of pressure ulcer development. Exton-Smith and Sherwin [23] conducted one study in a hospital geriatric unit and observed that 90% of elderly patients who made fewer than 10 movements over a seven-hour period developed a pressure ulcer. However, those who made at least 54 movements did not develop a pressure ulcer. Barbenel et al. [94] observed the movements of 40 hospital patients and showed that patients identified as being at risk of developing a pressure ulcer according to the Norton clinical assessment made a reduced number of movements. Additionally, spontaneous movements made by patients may be responsible for a temporary increase in skin blood flow, thereby reducing the risk of pressure ulceration [95].

The inability to re-position is especially crucial in patients who may have reduced mobility due to pharmacologic therapies (sedatives, analgesics etc), pain, or medical conditions or treatments that limit movement. These patients may all be impaired in their ability to reposition in response to discomfort from compressive forces. In particular mechanically ventilated, critically ill patients, who are placed in elevated backrest positions (>30°) to

reduce the incidence of ventilator associated pneumonia, and may have varying levels of alertness, may be at greater risk for pressure ulcer formation due to inability to reposition.

However, little is known about the effect of an individual's re-positioning ability based on their behavior state (alert, sedated) on pressure at the skin-bed interface, particularly in response to discomfort following changes in head-of-bed elevation. Therefore the specific aim of this section is to describe the effect of behavior state (alert, sedated) and backrest elevation on skin interface pressures. Using adult volunteers in a laboratory setting, skin interface pressure data were collected during simulated behavioral states reflective of those found in the critically ill (eg, alert or sedated) at varying degrees of backrest elevation.

6.2 Methods

6.2.1 Sample and Setting

The study was conducted in Virginia Commonwealth University, School of Nursing Clinical Learning Center. Study procedures were approved by the Institutional Review Board. A sample of 50 healthy participants was obtained from volunteers, 18 years of age or older. Exclusion criteria included sacral skin disorders, neuromuscular disorders (eg, cerebral palsy or Parkinson's disease), inability to move (eg, stroke), or inability to speak English. Self-reported demographic information was collected from the study participants (age, weight, height, and gender).

6.2.2 Procedures

Skin interface pressure was measured using the XSensor pressure sensing mat; subject behavior state was measured using actigraphy; and backrest elevation was measured using an inclinometer. The equipment is described in detail in Chapter 3.

Equipment was set up on a standard hospital bed and actigraphy watch was placed on the participant's non-dominant wrist. To ensure that each participant was in the same

body position in relation to the hospital bed's bending points, a calibration procedure was performed before data collection began. The calibration procedure required the backrest elevation to be raised to a 45°; the participant was asked to align their body's natural bending points with the bed's bending points; then, the bed was lowered.

During data collection, backrest elevation was increased to a randomly selected angle (30°/45°/60°) and the participant was asked to simulate a sedated state for 30 seconds. During a sedated state, the participant refrained from repositioning his or her body in response to discomfort.

The participant was then asked to simulate an alert state for 30 seconds. During an alert state, the participant could reposition his or her body until a comfortable position was reached. If the participant felt he or she was already in a comfortable position, then no repositioning was necessary. The head of bed was then lowered to a flat position. After a 30 second rest period, the procedure was repeated until all data for all three study angles were collected.

6.2.3 Data Analysis

Descriptive statistics were computed to describe the age, weight, height, and gender for the sample of participants. Segmentation was completed manually by an expert observer using a graphic user interface (GUI) created using MATLAB. Pressure images were segmented into 5 regions of interest that represent the body areas where skin interface pressure effects are most often seen when in a supine position: left scapula, right scapula, sacrum, left heel, and right heel. Descriptive statistics for pressure within the whole body and at each body segment were completed for each behavior state. Random effects models were used to examine the effects of operator and position on pressure. Predictor variables considered were condition (alert/sedated), angle (30°/45°/60°), the interaction between the two, BMI, actigraphy on the arm, contact area, total area, the upper leg and the lower leg angles. Statistical analysis was performed using (SAS/JMP).

Demographic		N	%
Gender	Male	9	18
	Female	41	82
Race	Asian	5	10
	Black or African American	5	10
	Whie	36	72
	Other	4	8
Ethnicity	Hispanic or Latino	1	2
	Not Hispanic or Latino	49	98
Variables		Mean	SD
Age (years)		30.04	10.98
Height (inches)		66.8	3.19
Weight (lbs)		155.78	38.51
BMI		24.39	4.93

Table 6.1: Demographic Data of Healthy Participants for Repositioning Study

6.3 Results

6.3.1 Participants

Fifty participants were recruited for this study. Participants were primarily young females, who were non-Hispanic, and white (Table 6.1).

6.3.2 Peak Pressure

Peak pressure measured across the whole body, sacrum, and heels generally increased with increased backrest elevation; peak pressure measured across the scapula generally decreased as backrest elevation increased (Figure 6.1). Peak pressure measured over the whole body was typically greater in the alert condition than the sedate condition (Figure 6.1a). There was a significant interaction between condition and angle as related to peak pressure ($p=0.0369$). Thus the differences in peak pressures between the states are not the same for all backrest elevation angles. Specifically, peak pressure differences between the conditions were greatest when backrest elevation was 45° and least when backrest elevation was 30°, as shown in

Figure 6.1a.

Peak pressure experienced at the sacrum tended to increase as backrest elevation increased (Figure 6.1b). Peak pressures at the sacrum were significantly greater during the alert condition at backrest elevations of 30° and 45°. At backrest elevation of 60°, there was no significant difference between the simulated states.

Peak pressures experienced at the right and left scapula tended to decrease as backrest elevation was increased (Figure 6.1c, 6.1d). Simulated condition had no significant effect on peak pressure on the left scapula at backrest elevations of 30° and 45°. Simulated condition had a significant, but relatively small, effect on peak pressure on the right scapula at backrest elevations of 30° and 45°, with alert condition peak pressures greater by 1.03 mmHg at 30° and 0.73 mmHg at 45°. When backrest elevation was 60°, there was a slight difference in both scapula, with alert condition peak pressures lower by 1.93 mmHg and 0.75 mmHg in left and right scapula, respectively.

Peak pressures experienced at the left and right heels were significantly less for the alert condition at backrest elevations of 45° and 60°. At backrest elevation of 30°, the left heel had slightly lower peak pressures during the alert state by 3 mmHg. However, the right heel showed no significant differences between peak pressures.

BMI was significantly related to peak pressure ($p<0.0001$). Specifically, a higher BMI was associated with a decrease in peak pressure. Age, weight, height, and gender did not have significant effects on peak pressure.

6.3.3 Average Pressure

Average pressures measured across the whole body tended to increase with increased backrest elevation. Average pressures were significantly greater for the alert condition. However, differences in average pressure were no more than ±1.0 mmHg such that, while statistically significant, they are not likely to be clinically relevant.

There was a significant interaction between condition and angle as related to average

pressure ($p<0.0001$). The higher the BMI, the higher the average pressure. Sedated subjects had lower average pressure at 30°, 45°, and 60° than alert subjects, though differences were smaller and non-significant at 60°. As angle increased, so did the average pressure for both alert and sedated subjects. Within subject type (alert versus sedated), average pressure at 45° was significantly larger than that for 30°, and average pressure at 60° was significantly larger than that for 45°. BMI was significantly related to average pressure ($p<0.0001$).

6.3.4 Additional Findings

BMI was found to be significantly related to both average pressure and peak pressure. For this reason, its effect on pressure within the different conditions was explored further. Observations were divided further into whether or not the participant was overweight (BMI>30). From this analysis, it was found that participants who were overweight experienced significantly lower peak pressures than participants with normal weight, as shown in Figure 6.2a. Participants who were overweight did not experience any statistically significant differences as a result of simulated condition; in other words, there was no difference in peak pressure depending on alert or sedated simulated condition. Participants with normal weight, however, had statistically significant differences between alert and sedated simulated conditions, especially as backrest elevation increased.

6.4 Discussion

Patient repositioning can play a crucial role in the prevention of pressure ulcers [96]. Typically, nurses reposition a patient in an effort to reduce skin interface pressures at bony prominences or to achieve interface pressures below a threshold of 32 mmHg. However, few studies have demonstrated the role of a patient's ability to self-position.

Volunteers experienced greater peak and average pressure across their whole body after they had re-positioned themselves. This contradicts the suggested hypothesis that self-

positioning is initiated in order to reduce pressure. This may demonstrate that interface pressure alone is a poor indicator of patient discomfort.

As supported by the literature, interface pressures tend to increase as backrest elevation increases [97, 55]. When individual body parts were segmented, the peak pressures occurring in the sacrum tended to increase with backrest elevation, while peak pressures in both scapula tended to decrease. This illustrates the tendency for pressure to be off-loaded from the scapula and instead distributed to the sacrum as the patient is elevated closer to a sitting position. In other words, pressure on the whole body increases with backrest elevation; however, some body parts decrease in pressure while others increase. This illustrates the importance of measuring pressure at different parts of the body in order to understand the effects of various clinical interventions on interface pressure.

Higher BMI led to higher average pressure, but lower peak pressure. This may indicate that those with higher BMI had better pressure distribution across their body area. This is similar to previous studies, in which low BMI is associated with increased pressure ulcer risk [98, 99, 100]. With regard to how peak pressure in the sacrum behaved with respect to changes in elevation or simulated state, each elevation increase showed a significant increase in peak pressure except within the sedated condition comparing 45° to 60°. In terms of average pressure across the sacrum, those observations in which an alert state was simulated were significantly greater than when a sedated state was simulated, for all backrest elevations. Regardless of simulated state, each elevation increase showed a significant increase in average pressure.

Peak pressure in scapula generally decreased as backrest elevation increased; however, these decreases were significant for both right and left scapula only within the observations of a simulated alert state, when comparing 45° to 60° and 30° to 60°. Peak pressures collected during a simulated sedate state were generally greater than those collected during an alert state. When participants were in an alert state, sacrum peak pressures tended to be greater than during the sedated state, but scapula peak pressures tended to be lesser. This indicates

that participants may have felt more comfortable distributing pressure largely across their sacrum in order to relieve pressure applied to their scapula.

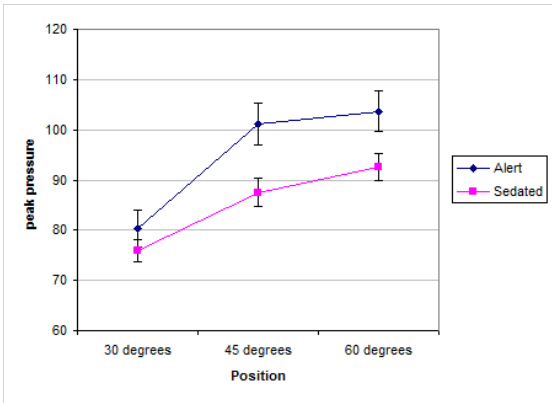

(a) Whole body

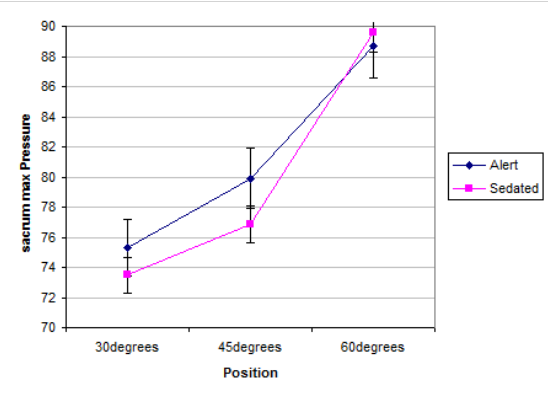

(b) Sacrum

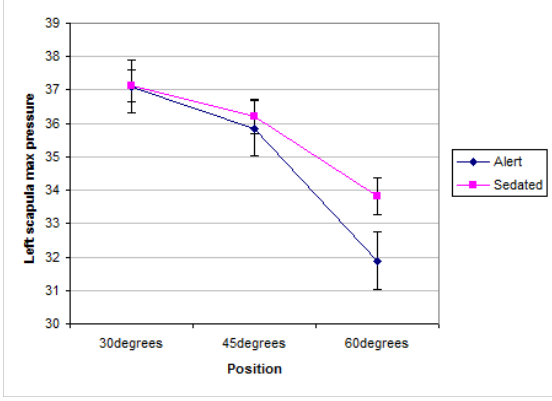

(c) Left Scapula

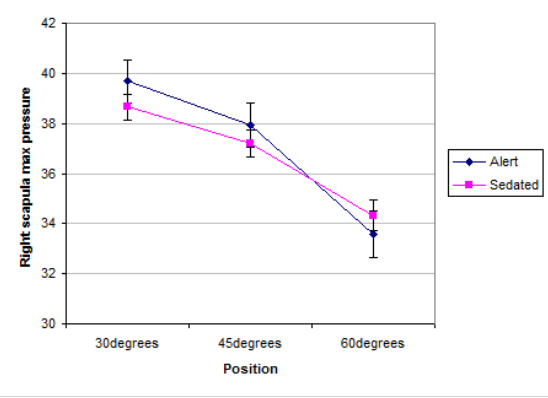

(d) Right Scapula

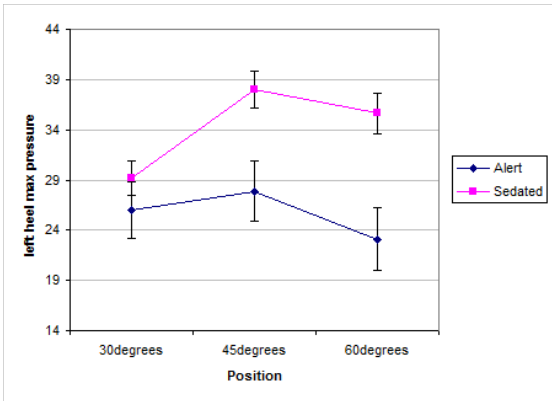

(e) Left Heel

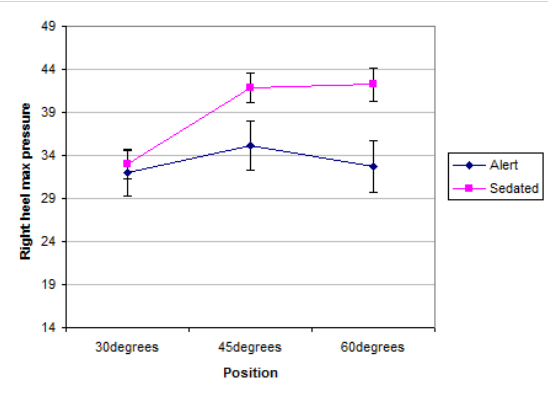

(f) Right Heel

Figure 6.1: Effect of backrest elevation on peak pressure

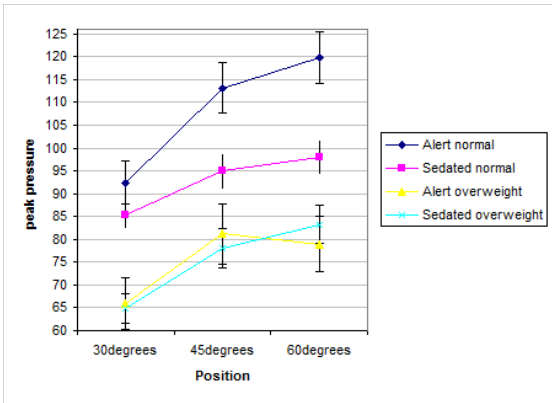

(a) Whole body

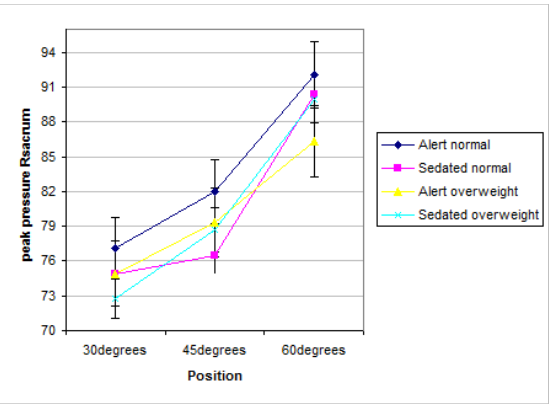

(b) Sacrum

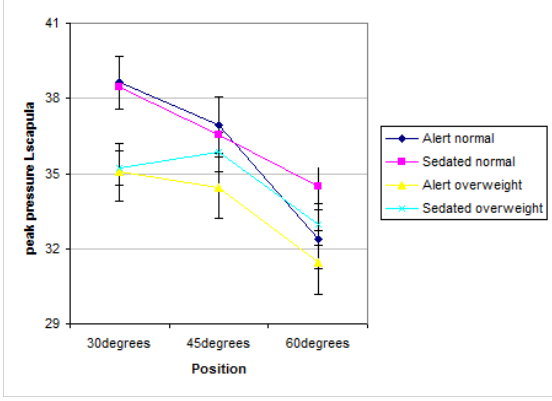

(c) Left Scapula

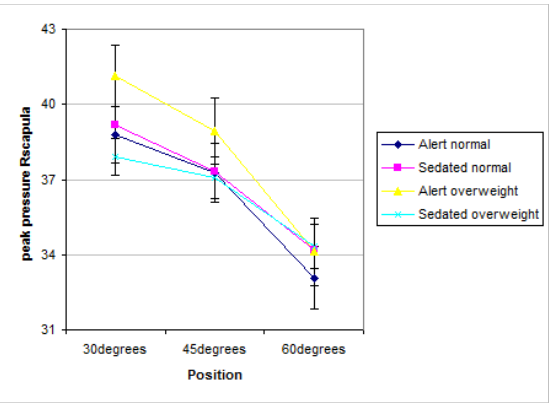

(d) Right Scapula

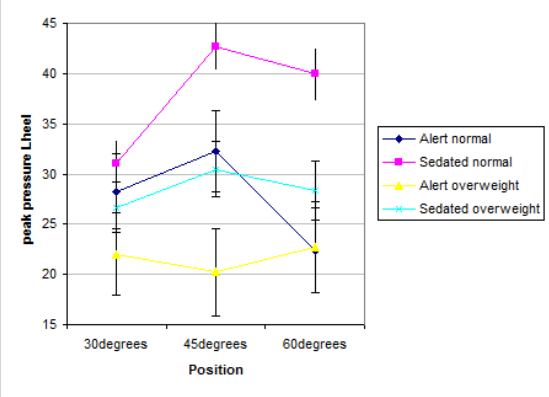

(e) Left Heel

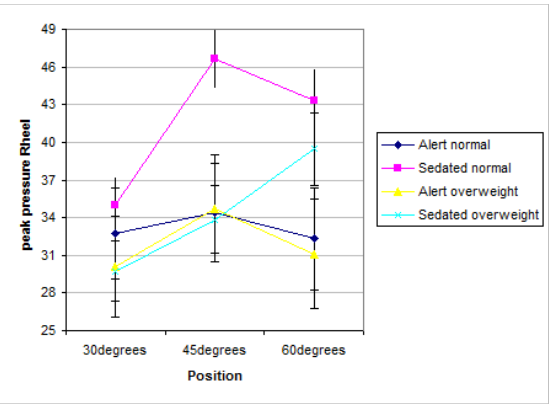

(f) Right Heel

Figure 6.2: Effect of Body Mass Index (BMI) on peak pressure

Chapter 7

Conclusions

7.1 Summary

Pressure ulcers are a persistent health care concern of national significance, with an estimated yearly cost of $3 billion in the United States alone. Reducing interface pressure remains one of the most effective methods for reducing pressure ulcer incidence and severity. However, studying the effect of interface pressure on pressure ulcer development in a hospital setting has proven difficult. Pressure ulcers may develop after several days of hospitalization; therefore, the study of pressure ulcer development may require several days of continuous monitoring. Such monitoring results in an enormous amount of acquired data, which can be difficult to interpret. Furthermore, continuous data acquisition in a critical-care setting is a difficult task in itself and patient motion is often sporadic and non-periodic.

The presented research applies human motion analysis techniques in order to automatically segment pressure images acquired in a hospital setting. The algorithm determines patient pose with a traditional classification algorithm. A model-based approach is applied to the acquired pressure image and the image is segmented into clinically relevant regions of interest. The algorithm is robust to some instances of occlusion as well as certain cases of the object of interest exiting the sensing area.

The dissertation presented here makes the following contributions to the area of pressure ulcer research:

- Provides a reliable method for classifying patient pose in a hospital setting. This method can be used to study the efficacy of turning operations in pressure ulcer development.

- Presents an automatic segmentation algorithm specifically designed for marking clinically relevant regions of interest. The algorithm can be used in a hospital setting and is the most complete algorithm to date for use in pressure ulcer studies.

- Demonstrates the importance of segmenting pressure images into regions of interest. Additionally, the study with healthy volunteers provides some insight as to how such risk factors as immobility and BMI might affect pressure ulcer development.

7.2 Future Work

While the presented work provides a robust automatic segmentation method, future work can improve the algorithm's performance. Potential areas include:

- Exploring the use of bottom-up approaches. Bottom-up approaches have been used to identify strong image features, which are assumed to be body parts. Recently, human motion analysis has made advances in combination techniques that take advantage of the good qualities of both bottom-up and top-down approaches.

  A possible way of incorporating the technique into the presented algorithm may be to use a bottom-up approach to improve the locating of image extremities. The head and feet can be assumed to have strong identifying characteristics. In the absence of finding the head and feet using a bottom-up approach, the algorithm can revert to the presented method of finding extremities. Conversely, the algorithm can assume that those parts are not included in the sensing area and act accordingly. This amendment

may also improve performance by making the algorithm better able to handle unusual instances when the head and feet are off the bed.

- Improving algorithm performance. One of the major issues with algorithm performance was the assumption that the patient's head and heels were present on the pressure sensing area. However, this was not always the case. A solution to this problem might be to have several kinematic models and decide beforehand which model is the most appropriate to apply to the image. The integral histogram is a popular method to speed up computer vision tasks. Implementing this algorithm may be effective in deciding whether the patient's head and heels are present in the image and deciding which model (head-less or normal) is more appropriate for applying to the image.

- Allowing manual input of patient data. Using patient height may help the algorithm achieve better results. Additionally, the algorithm does not yet handle cases where patients who have undergone amputation.

- Reducing the average image processing time. Currently, the computational cost of the algorithm prohibits its use in a real-time application. One possibility for improving processing speed may be to translate the algorithm into a different programming language. However, MATLAB code is optimized for matrices, which lends itself well to image analysis. Therefore, it is uncertain how much speed can be gained from an alternate programming language. Additionally, the use of parallel computing has not yet been explored.

- Improving kinematic constraints. There were a few instances when the optimization algorithm proposed an improbable pose in order to explain the image. Improving the kinematic constraints of the model (i.e., improved enforcing of joint angles) may lead to better overall performance. However, this will add complexity to the model, and increased computation time may be sacrificed for improved performance.

- Implementing a motion tracking algorithm. Motion tracking algorithms gain efficacy in the presence of strong image descriptors and/or periodic motion. Because these are not valid assumptions for the acquired pressure images, such methods were not initially used for the algorithm. However, an effective use of a motion tracking algorithm may be to initialize the model using the algorithm described here, then use the motion tracking algorithm to speed image analysis for consecutive frames.

- Implementing algorithm directly into the XSensor software. Currently, XSensor does not even support exporting data into MATLAB files. Even with this software change, algorithm speed-up is possible. As the need for pressure ulcer research grows, however, it may be beneficial for XSensor to implement automatic segmentation into their proprietary software.

Additionally, this algorithm's application extends to several other areas, including:

- Use in studies to determine the importance of potential risk factors. The role of age and nutrition are still not well understood; pressure image studies may be used to determine if the pressure-time threshold changes with respect to these factors. The segmentation algorithm can be used to determine if certain regions of the body are more greatly influenced compared to other areas.

- Use to determine the efficacy of clinical interventions for pressure ulcers. In this dissertation, an individual's ability to re-positioning was explored, and then extended to the global impact of patient mobility. Other clinical interventions that can be explored are: the effectiveness of turning operation, heel protective devices, continuous lateral rotation therapy (CLRT), or the positioning of pillows and wedges. There may also be the potential for further studying patient mobility through the ability to discern between spontaneous patient-initiated movement and turning operation initiated by hospital staff.

- Use in other pressure imaging applications. The presented algorithm is relatively simple and easily adaptable to other applications that involve analyzing the movements of an articulated model.

Bibliography

[1] K. Beckrich and S.A. Aronovitch. Hospital-acquired pressure ulcers: A comparison of costs in medical versus surgical patients. *Advances in Skin & Wound Care*, 11:3, 1998.

[2] K. Vanderwee, T. Defloor, D. Beeckman, L. Demarré, S. Verhaeghe, T. Van Durme, and M. Gobert. Assessing the adequacy of pressure ulcer prevention in hospitals: a nationwide prevalence survey. *BMJ Quality & Safety*, 20(3):260–267, 2011.

[3] G. Bours, E. Laat, R. Halfens, and M. Lubbers. Prevalence, risk factors and prevention of pressure ulcers in dutch intensive care units. *Intensive care medicine*, 27(10):1599–1605, 2001.

[4] J.G. Cuddigan, E.A. Ayello, C. Sussman, and S. Baranoski. *Pressure ulcers in America: prevalence, incidence, and implications for the future*. National Pressure Ulcer Advisory Panel, 2001.

[5] C Allison Russo, Claudia Steiner, and William Spector. Hospitalizations related to pressure ulcers among adults 18 years and older, 2006. 2008.

[6] E.A. Ayello and C.H. Lyder. A new era of pressure ulcer accountability in acute care. *Advances in skin & wound care*, 21(3):134–140, 2008.

[7] Wound rounds: Common areas for pressure ulcers.

[8] N. Bergstrom. *Patients at risk for pressure ulcers and evidence-based care for pressure ulcer prevention*, pages 35–50. Springer.

[9] Prevention of pressure ulcers: Quick reference guide.

[10] C.V. Bouten, C.W. Oomens, F.P. Baaijens, and D.L. Bader. The etiology of pressure ulcers: skin deep or muscle bound? *Archives of physical medicine and rehabilitation*, 84(4):616–619, 2003.

[11] C. VanGilder, S. Amlung, P. Harrison, and S. Meyer. Results of the 2008-2009 international pressure ulcer prevalence survey and a 3-year, acute care, unit-specific analysis. *Ostomy wound management*, 55(11):39–45, 2009.

[12] J.M. Black et al. Moving toward consensus on deep tissue injury and pressure ulcer staging. *Advances in Skin & Wound Care*, 18(8):415–421, 2005.

[13] Pressure ulcer category/staging illustrations.

[14] B. Braden and N. Bergstrom. A conceptual schema for the study of the etiology of pressure sores. *Rehabilitation nursing : the official journal of the Association of Rehabilitation Nurses*, 12(1):8–12, Jan-Feb 1987.

[15] T. Defloor. The risk of pressure sores: a conceptual scheme. *Journal of clinical nursing*, 8(2):206–216, 1999.

[16] Pedro L Pancorbo-Hidalgo, Francisco Pedro Garcia-Fernandez, Isabel Ma Lopez-Medina, and Carmen Alvarez-Nieto. Risk assessment scales for pressure ulcer prevention: a systematic review. *Journal of advanced nursing*, 54(1):94–110, 2006.

[17] J Waterlow. A risk assessment card. *Nursing Times*, 81(48):49–56, 1985.

[18] Davina J Gosnell. An assessment tool to identify pressure sores. *Nursing research*, 22(1):55–58, 1973.

[19] Doreen Norton. Calculating the risk. reflections on the norton scale. *Advances in Skin & Wound Care*, 2(3):24–31, 1989.

[20] Elizabeth A Ayello and Barbara Braden. How and why to do pressure ulcer risk assessment. *Advances in Skin & Wound Care*, 15(3):125–131, 2002.

[21] DJ Gosnell. Pressure sore risk assessment. part ii. analysis of risk factors. *Decubitus*, 2(3):40, 1989.

[22] FX Keane. The minimum physiological mobility requirement for man supported on a soft surface. *Spinal Cord*, 16(4):383–389, 1979.

[23] Exton-Smith An, Sherwin Rw, et al. The prevention of pressure sores. significance of spontaneous bodily movements. *Lancet*, 2(7212):1124, 1961.

[24] Panos Papanikolaou, Patricia A Lyne, and Emma J Lycett. Pressure ulcer risk assessment: application of logistic analysis. *Journal of advanced nursing*, 44(2):128–136, 2003.

[25] Yoshio Mino, Shigeto Morimoto, Kohya Okaishi, Shoroku Sakurai, Miyuki Onishi, Masashi Okuro, Akiko Matsuo, and Toshio Ogihara. Risk factors for pressure ulcers in bedridden elderly subjects: Importance of turning over in bed and serum albumin level. *Geriatrics & Gerontology International*, 1(1-2):38–44, 2001.

[26] David J Margolis, Warren Bilker, Jill Knauss, Mona Baumgarten, and Brian L Strom. The incidence and prevalence of pressure ulcers among elderly patients in general medical practice. *Annals of epidemiology*, 12(5):321–325, 2002.

[27] Kathy Whittington, Martha Patrick, and Joan L Roberts. A national study of pressure ulcer prevalence and incidence in acute care hospitals. *Journal of Wound Ostomy & Continence Nursing*, 27(4):209–215, 2000.

[28] Nicholas Graves, Frances Birrell, and Michael Whitby. Effect of pressure ulcers on length of hospital stay. *Infection control and hospital epidemiology*, 26(3):293–297, 2005.

[29] Becky Dorner, Mary Ellen Posthauer, David Thomas, et al. The role of nutrition in pressure ulcer prevention and treatment: National pressure ulcer advisory panel white paper. *Advances in skin & wound care*, 22(5):212–221, 2009.

[30] CH Lyder, C Yu, D Stevenson, R Mangat, O Empleo-Frazier, J Emerling, and J McKay. Validating the braden scale for the prediction of pressure ulcer risk in blacks and latino/hispanic elders: a pilot study. *Ostomy/wound management*, 44(3A Suppl):42S, 1998.

[31] Susan D Horn, Stacy A Bender, Maree L Ferguson, Randall J Smout, Nancy Bergstrom, George Taler, Abby S Cook, Siobhan S Sharkey, and Anne Coble Voss. The national pressure ulcer long-term care study: Pressure ulcer development in long-term care residents. *Journal of the American Geriatrics Society*, 52(3):359–367, 2004.

[32] Shirley A Gilmore, Gretchen Robinson, Mary Ellen Posthauer, and Janice Raymond. Clinical indicators associated with unintentional weight loss and pressure ulcers in elderly residents of nursing facilities. *Journal of the American Dietetic Association*, 95(9):984–992, 1995.

[33] Catherine VanGilder, Gordon MacFarlane, Stephanie Meyer, and Charlie Lachenbruch. Body mass index, weight, and pressure ulcer prevalence: An analysis of the 2006-2007 international pressure ulcer prevalence (tm) surveys. *Journal of nursing care quality*, 24(2):127–135, 2009.

[34] Leon Bennett and Bok Y Lee. Pressure versus shear in pressure sore causation. *Chronic ulcers of the skin. McGraw Hill New York*, 1985.

[35] J Bridel. The aetiology of pressure sores. *J Wound Care*, 2(4):230–238, 1993.

[36] Steven Antokal, David Brienza, Nancy Bryan, Laura Herbe, Susan Logan, Jeanine Maguire, Kathy Strang, Maranda Vanbruaene, Jennifer Van Ranst, and Aamir Sid-

diqui. Friction induced skin injuries–are they pressure ulcers? a national pressure ulcer advisory panel white paper. 2012.

[37] SM Dinsdale. Decubitus ulcers: role of pressure and friction in causation. *Archives of physical medicine and rehabilitation*, 55(4):147, 1974.

[38] KE Groth. Clinical observations and experimental studies of the pathogenesis of decubitus ulcers. *Acta Chir Scand*, 76(1):209, 1942.

[39] T. Husain. An experimental study of some pressure effects on tissues, with reference to the bed-sore problem. *The Journal of pathology and bacteriology*, 66(2):347–358, 1953.

[40] M. Kosiak et al. Etiology and pathology of ischemic ulcers. *Archives of Physical Medicine and Rehabilitation*, 40(2):62, 1959.

[41] JB Reswick and JE Rogers. *Experience at Rancho Los Amigos Hospital with devices and techniques to prevent pressure sores*, pages 301–310. Baltimore, MD: University Park Press, 1976.

[42] A. GEFEN. Reswick and rogers pressure-time curve for pressure ulcer risk. part 1. *Nursing standard*, 23(45), 2009.

[43] T. Defloor and J.D.S. De Schuijmer. Preventing pressure ulcers: An evaluation of four operating-table mattresses. *Applied Nursing Research*, 13(3):134–141, 2000.

[44] M.G. Kemp, J.K. Keithley, D.W. Smith, and B. Morreale. Factors that contribute to pressure sores in surgical patients. *Research in nursing & health*, 13(5):293–301, 2007.

[45] E. Linder-Ganz, N. Shabshin, Y. Itzchak, Z. Yizhar, I. Siev-Ner, and A. Gefen. Strains and stresses in sub-dermal tissues of the buttocks are greater in paraplegics than in healthy during sitting. *Journal of biomechanics*, 41(3):567–580, 2008.

[46] A. Gefen, B. van Nierop, D.L. Bader, and C.W. Oomens. Strain-time cell-death threshold for skeletal muscle in a tissue-engineered model system for deep tissue injury. *Journal of biomechanics*, 41(9):2003–2012, 2008.

[47] A.H. Sacks. Theoretical prediction of a time-at-pressure curve for avoiding pressure sores. *J Rehabil Res Dev*, 26(3):27–34, 1989.

[48] A. Gefen et al. Reswick and rogers pressure-time curve for pressure ulcer risk. part 2. *Nursing standard (Royal College of Nursing (Great Britain): 1987)*, 23(46):40, 2009.

[49] Frederick Shelton, Richard Barnett, and Eric Meyer. Full-body interface pressure testing as a method for performance evaluation of clinical support surfaces. *Applied ergonomics*, 29(6):491–497, 1998.

[50] Jasper Reenalda, Paul Geffen, Marc Nederhand, Michiel Jannink, Maarten IJzerman, and Hans Rietman. Analysis of healthy sitting behavior: interface pressure distribution and subcutaneous tissue oxygenation. *Journal of Rehabilitation Research & Development*, 46(5):577–586, 2009.

[51] JB Hardin, SN Cronin, and K Cahill. Comparison of the effectiveness of two pressure-relieving surfaces: low-air-loss versus static fluid. *Ostomy/wound management*, 46(9):50, 2000.

[52] BPJA Keller, PHW Lubbert, E Keller, and LPH Leenen. Tissue-interface pressures on three different support-surfaces for trauma patients. *Injury*, 36(8):946–948, 2005.

[53] Patricia G Turpin and Valerie Pemberton. Prevention of pressure ulcers in patients being managed on clrt: Is supplemental repositioning needed? *Journal of Wound Ostomy & Continence Nursing*, 33(4):381–388, 2006.

[54] Kozue Sakai, Hiromi Sanada, Noriko Matsui, Gojiro Nakagami, Junko Sugama, Chieko Komiyama, and Naoki Yahagi. Continuous monitoring of interface pressure distri-

bution in intensive care patients for pressure ulcer prevention. *Journal of advanced nursing*, 65(4):809–817, 2009.

[55] Maki Mimura, Takehiko Ohura, Makoto Takahashi, Ryuji Kajiwara, and Norihiko Ohura Jr. Mechanism leading to the development of pressure ulcers based on shear force and pressures during a bed operation: influence of body types, body positions, and knee positions. *Wound Repair and Regeneration*, 17(6):789–796, 2009.

[56] Jake K Aggarwal and Qin Cai. Human motion analysis: A review. In *Nonrigid and Articulated Motion Workshop, 1997. Proceedings., IEEE*, pages 90–102. IEEE, 1997.

[57] Thomas B Moeslund and Erik Granum. A survey of computer vision-based human motion capture. *Computer Vision and Image Understanding*, 81(3):231–268, 2001.

[58] Dariu M Gavrila. The visual analysis of human movement: A survey. *Computer vision and image understanding*, 73(1):82–98, 1999.

[59] Ronald Poppe. Vision-based human motion analysis: An overview. *Computer Vision and Image Understanding*, 108(1):4–18, 2007.

[60] Ramprasad Polana and Randal Nelson. Low level recognition of human motion (or how to get your man without finding his body parts). In *Motion of Non-Rigid and Articulated Objects, 1994., Proceedings of the 1994 IEEE Workshop on*, pages 77–82. IEEE, 1994.

[61] Junji Yamato, Jun Ohya, and Kenichiro Ishii. Recognizing human action in time-sequential images using hidden markov model. In *Computer Vision and Pattern Recognition, 1992. Proceedings CVPR'92., 1992 IEEE Computer Society Conference on*, pages 379–385. IEEE, 1992.

[62] Rick Kjeldsen and John Kender. Toward the use of gesture in traditional user interfaces. In *Automatic Face and Gesture Recognition, 1996., Proceedings of the Second International Conference on*, pages 151–156. IEEE, 1996.

[63] Shannon X Ju, Michael J Black, and Yaser Yacoob. Cardboard people: A parameterized model of articulated image motion. In *Automatic Face and Gesture Recognition, 1996., Proceedings of the Second International Conference on*, pages 38–44. IEEE, 1996.

[64] Navneet Dalal and Bill Triggs. Histograms of oriented gradients for human detection. In *Computer Vision and Pattern Recognition, 2005. CVPR 2005. IEEE Computer Society Conference on*, volume 1, pages 886–893. IEEE, 2005.

[65] Ankur Agarwal and Bill Triggs. A local basis representation for estimating human pose from cluttered images. *Computer Vision–ACCV 2006*, pages 50–59, 2006.

[66] Ryuzo Okada and Stefano Soatto. Relevant feature selection for human pose estimation and localization in cluttered images. *Computer Vision–ECCV 2008*, pages 434–445, 2008.

[67] Ming-Kuei Hu. Visual pattern recognition by moment invariants. *Information Theory, IRE Transactions on*, 8(2):179–187, 1962.

[68] Jan Flusser. On the independence of rotation moment invariants. *Pattern Recognition*, 33(9):1405–1410, 2000.

[69] Jan Flusser and Tomáš Suk. Rotation moment invariants for recognition of symmetric objects. *Image Processing, IEEE Transactions on*, 15(12):3784–3790, 2006.

[70] David G Lowe. Method and apparatus for identifying scale invariant features in an image and use of same for locating an object in an image, March 23 2004. US Patent 6,711,293.

[71] Ryuji Funayama, Hiromichi Yanagihara, Luc Van Gool, Tinne Tuytelaars, and Herbert Bay. Robust interest point detector and descriptor, June 9 2010. EP Patent 1,850,270.

[72] Russell Cork. Xsensor technology: a pressure imaging overview. *Sensor Review*, 27(1):24–28, 2007.

[73] Xsensor sensor specification sheet: X3 px100:48:144.02.

[74] Mary Jo Grap, Virginia A Hamilton, Ann McNallen, Jessica M Ketchum, Al M Best, Nyimas Y Isti Arief, and Paul A Wetzel. Actigraphy: Analyzing patient movement. *Heart & Lung: The Journal of Acute and Critical Care*, 40(3):e52–e59, 2011.

[75] T. Harada, T. Mori, Y. Nishida, T. Yoshimi, and T. Sato. Body parts positions and posture estimation system based on pressure distribution image. In *Robotics and Automation, 1999. Proceedings. 1999 IEEE International Conference on*, volume 2, pages 968–975. IEEE, 1999.

[76] Tatsuya Harada, Tomomasa Sato, and Taketoshi Mori. Human motion tracking system based on skeleton and surface integration model using pressure sensors distribution bed. In *Human Motion, 2000. Proceedings. Workshop on*, pages 99–106. IEEE, 2000.

[77] T. Harada, T. Sato, and T. Mori. Pressure distribution image based human motion tracking system using skeleton and surface integration model. In *Robotics and Automation, 2001. Proceedings 2001 ICRA. IEEE International Conference on*, volume 4, pages 3201–3207. IEEE, 2001.

[78] R Yousefi, S Ostadabbas, M Faezipour, M Farshbaf, M Nourani, L Tamil, and M Pompeo. Bed posture classification for pressure ulcer prevention. In *Engineering in Medicine and Biology Society, EMBC, 2011 Annual International Conference of the IEEE*, pages 7175–7178. IEEE, 2011.

[79] R Yousefi, S Ostadabbas, M Faezipour, M Nourani, V Ng, L Tamil, A Bowling, D Behan, and M Pompeo. A smart bed platform for monitoring & ulcer prevention. In *Biomedical Engineering and Informatics (BMEI), 2011 4th International Conference on*, volume 3, pages 1362–1366. IEEE, 2011.

[80] Sarah Ostadabbas, Rasoul Yousefi, Miad Faezipour, Mehrdad Nourani, and Matthew Pompeo. Pressure ulcer prevention: An efficient turning schedule for bed-bound patients. In *Life Science Systems and Applications Workshop (LiSSA), 2011 IEEE/NIH*, pages 159–162. IEEE, 2011.

[81] S Ostadabbas, R Yousefi, M Nourani, M Faezipour, L Tamil, and M Pompeo. A resource-efficient planning for pressure ulcer prevention. 2012.

[82] R. Grimm, J. Sukkau, J. Hornegger, and G. Greiner. Automatic patient pose estimation using pressure sensing mattresses. *Bildverarbeitung für die Medizin 2011*, pages 409–413, 2011.

[83] R. Grimm, S. Bauer, J. Sukkau, J. Hornegger, and G. Greiner. Markerless estimation of patient orientation, posture and pose using range and pressure imaging. *International journal of computer assisted radiology and surgery*, pages 1–9, 2012.

[84] Martin T Hagan and Mohammad B Menhaj. Training feedforward networks with the marquardt algorithm. *Neural Networks, IEEE Transactions on*, 5(6):989–993, 1994.

[85] CC Hsia, KJ Liou, APW Aung, V Foo, W Huang, and J Biswas. Analysis and comparison of sleeping posture classification methods using pressure sensitive bed system. In *Engineering in Medicine and Biology Society, 2009. EMBC 2009. Annual International Conference of the IEEE*, pages 6131–6134. IEEE, 2009.

[86] Merck manual for health care professionals online. physical therapy. `http://www.merckmanuals.com/professional/special_subjects/rehabilitation/physical_therapy_pt.html`, 2012.

[87] Jeffrey C Lagarias, James A Reeds, Margaret H Wright, and Paul E Wright. Convergence properties of the nelder–mead simplex method in low dimensions. *SIAM Journal on Optimization*, 9(1):112–147, 1998.

[88] Alexandru O Balan, Leonid Sigal, Michael J Black, James E Davis, and Horst W Haussecker. Detailed human shape and pose from images. In *Computer Vision and Pattern Recognition, 2007. CVPR'07. IEEE Conference on*, pages 1–8. IEEE, 2007.

[89] Lynda D Copeland-Fields and Barbara R Hoshiko. Clinical validation of braden and bergstrom's conceptual schema of pressure sore risk factors. *Rehabilitation Nursing*, 14(5):257–260, 1989.

[90] Richard M Allman, Patricia S Goode, Martha M Patrick, Nickie Burst, and Alfred A Bartolucci. Pressure ulcer risk factors among hospitalized patients with activity limitation. *JAMA: the journal of the American Medical Association*, 273(11):865–870, 1995.

[91] Nancy Bergstrom, Barbara Braden, Mildred Kemp, Mary Champagne, Elizabeth Ruby, et al. Multi-site study of incidence of pressure ulcers and the relationship between risk level, demographic characteristics, diagnoses, and prescription of preventive interventions. *Journal of the American Geriatrics Society*, 44(1):22–30, 1996.

[92] Yoshio Mino, Shigeto Morimoto, Kohya Okaishi, Shoroku Sakurai, Miyuki Onishi, Masashi Okuro, Akiko Matsuo, and Toshio Ogihara. Risk factors for pressure ulcers in bedridden elderly subjects: Importance of turning over in bed and serum albumin level. *Geriatrics & Gerontology International*, 1(1-2):38–44, 2001.

[93] Margareta Lindgren, Mitra Unosson, Mats Fredrikson, and Anna-Christina Ek. Immobility–a major risk factor for development of pressure ulcers among adult hospitalized patients: a prospective study. *Scandinavian Journal of Caring Sciences*, 18(1):57–64, 2004.

[94] JC Barbenel, MW Ferguson-Pell, and AQ Beale. Monitoring the mobility of patients in bed. *Medical and Biological Engineering and Computing*, 23(5):466–468, 1985.

[95] V Schubert and J Heraud. The effects of pressure and shear on skin microcirculation in elderly stroke patients lying in supine or semi-recumbent positions. *Age and ageing*, 23(5):405–410, 1994.

[96] Toshiko Kaitani, Keiko Tokunaga, Noriko Matsui, and Hiromi Sanada. Risk factors related to the development of pressure ulcers in the critical care setting. *Journal of clinical nursing*, 19(3-4):414–421, 2010.

[97] M Peterson, W Schwab, K McCutcheon, J H van Oostrom, N Gravenstein, and L Caruso. Effects of elevating the head of bed on interface pressure in volunteers. *Critical care medicine*, 36(11):3038–3042, 2008.

[98] Mona Baumgarten, David J Margolis, A Russell Localio, Sarah H Kagan, Robert A Lowe, Bruce Kinosian, John H Holmes, Stephanie B Abbuhl, William Kavesh, and Althea Ruffin. Pressure ulcers among elderly patients early in the hospital stay. *The Journals of Gerontology Series A: Biological Sciences and Medical Sciences*, 61(7):749–754, 2006.

[99] Bette Olson, Diane Langemo, Christine Burd, Darlene Hanson, Susan Hunter, and Tressa Cathcart-Silberberg. Pressure ulcer incidence in an acute care setting. *Journal of WOCN*, 23(1):15–22, 1996.

[100] Margareta Lindgren, Mitra Unosson, Ann-Margret Krantz, and Anna-Christina Ek. Pressure ulcer risk factors in patients undergoing surgery. *Journal of advanced nursing*, 50(6):605–612, 2005.

[101] Jyh-Shing Roger Jang, Chuen-Tsai Sun, and Eiji Mizutani. *Neuro-fuzzy and soft computing: a computational approach to learning and machine intelligence*. PHI Learning, 2010.

Appendix A

Ellipses

An ellipse is a planar curve that results from the intersection of a cone by a plane in a way that produces a closed curve. The equation of an ellipse centered at the origin and whose major and minor axes coincide with the Cartesian axes is

$$\frac{x^2}{a^2} + \frac{y^2}{b^2} = 1 \tag{A.1}$$

The radius in the x-direction is a and in the y-direction is b. The longer of the two radii is known as the semi-major axis length and the other is the semi-minor axis length.

In matrix quadratic form, the equation for an ellipse A.1 can be written as

$$\begin{pmatrix} x & y \end{pmatrix} \begin{pmatrix} \frac{1}{a^2} & 0 \\ 0 & \frac{1}{b^2} \end{pmatrix} \begin{pmatrix} x \\ y \end{pmatrix} = 1 \tag{A.2}$$

$$\mathbf{x}^\intercal \begin{pmatrix} \frac{1}{a^2} & 0 \\ 0 & \frac{1}{b^2} \end{pmatrix} \mathbf{x} = 1 \tag{A.3}$$

$$\mathbf{x}^\intercal \mathbf{E}^{-1} \mathbf{x} = 1 \tag{A.4}$$

In the most general form $\mathbf{E}$ is a symmetrix matrix

$$\mathbf{E} = \begin{pmatrix} A & C \\ C & B \end{pmatrix} \tag{A.5}$$

and its determinant $\det(\mathbf{E}) = AB - C^2$ defines the type of conic

$$\det \mathbf{E} \begin{cases} > 0 & \text{ellipse} \\ = 0 & \text{parabola} \\ < 0 & \text{hyperbola} \end{cases} \tag{A.6}$$

Non-zero values of C change the orientation of the ellipse. The ellipse can be arbitrarily centered at x_c by writing it in the form

$$(x - x_c)^\intercal \mathbf{E}^{-1} (x - x_c) = 1 \tag{A.7}$$

Since $\mathbf{E}$ is symmetrix it can be rewritten as

$$\mathbf{E} = \mathbf{X} \Lambda \mathbf{X}^\intercal \tag{A.8}$$

where $\mathbf{X}$ is an orthogonal matrix comprising the eigenvectors of $\mathbf{E}$.

Conversely, equation A.7 can be represented in polynomial form by considering the equation of the form

$$(\mathbf{x} - (x_0, y_0))^\intercal \begin{pmatrix} a & c \\ c & b \end{pmatrix} (\mathbf{x} - (x_0, y_0)) = 1 \tag{A.9}$$

and expanding to obtain

$$e_1 x^2 + e_2 y^2 + e_3 xy + e_4 x + e_5 y + e_6 = 0 \tag{A.10}$$

where $e_1 = a, e_2 = b, e_3 = 2c, e_4 = -2(ax_0 + cy_0), e_5 = -2(by_0 + cx_0)$, and $e_6 = ax_0^2 + by_0^2 + 2cx_0y_y - 1$. The ellipse has only five degrees of freedom, its center coordinate and three unique elements in $\mathbf{E}$. For a non-degenerate ellipse $e_1 \neq 0$ and equation A.10 can be rewritten in normalized form

$$x^2 + E_1y^2 + E_2xy + E_3x + E_4y + E_5 = 0 \tag{A.11}$$

such that the polynomial equation for the ellipse has only five unique parameters.

A.1 Fitting an Ellipse to a Set of Boundary Points

Given a set of points (x_i, y_i) that define the boundary of an ellipse, the polynomial form of the ellipse given by A.11 can be used such that

$$\begin{pmatrix} y_1^2 & x_1y_1 & x_1 & y_1 & 1 \\ y_2^2 & x_2y_2 & x_2 & y_2 & 1 \\ & & \vdots & & \\ y_N^2 & x_Ny_N & x_N & y_N & 1 \end{pmatrix} \begin{pmatrix} E_1 \\ E_2 \\ E_3 \\ E_4 \\ E_5 \end{pmatrix} = \begin{pmatrix} -x_1^2 \\ -x_2^2 \\ \vdots \\ -x_N^2 \end{pmatrix} \tag{A.12}$$

The above equation is solvable for $N \geq 5$.

Appendix B

Nelder-Mead Simplex Algorithm

MATLAB's built-in function fminsearch uses the Nelder-Mead simplex method as described in Lagarias et al. [87]. The Nelder-Mead simplex algorithm is a derivative-free optimization method, which minimizes a real-valued function $f(x)$for $x \in \mathbb{R}^n$. The Nelder-Mead considers search-space parameters as the vertices of a simplex, a geometric object determined by an assembly of $n+1$ points, $p_0, p_1, \cdots, p_n$, in the n-dimensional space such that

$$\det \begin{bmatrix} p_0 & p_1 & \cdots & p_n \\ 1 & 1 & \cdots & 1 \end{bmatrix} \neq 0 \tag{B.1}$$

This condition ensures that two points in $\mathbb{R}$ do not coincide, three points in $\mathbb{R}^2$ are not colinear, four points in $\mathbb{R}^3$, and so on. Thus, a simplex in $\mathbb{R}$ is a line segment, in $\mathbb{R}^2$ is a triangle, and in $\mathbb{R}^3$ is a tetrahedron.

The algorithm initializes a simplex of $n+1$ vertices in n dimensions. A possible way to set up a simplex [101] is to start wtih an initial point $x^{(0)} = p_0$ and generate the remaining points of the initial simplex as

$$p_i = p_0 + \lambda_i e_i, i = 1, 2, \ldots, n \tag{B.2}$$

where the e_i are the natural basis for $(R)^n$, such that

$$e_1 = \begin{bmatrix} 1 \\ 0 \\ 0 \\ \vdots \\ 0 \\ 0 \end{bmatrix}, e_2 = \begin{bmatrix} 0 \\ 1 \\ 0 \\ \vdots \\ 0 \\ 0 \end{bmatrix}, \cdots, e_n = \begin{bmatrix} 0 \\ 0 \\ 0 \\ \vdots \\ 0 \\ 1 \end{bmatrix} \tag{B.3}$$

The positive constant coefficients λ_i are selected in such a way that their magnitudes reflect the length scale of the optimization problem.

In MATLAB, the algorithm creates the simplex around the user-provided initial guess p_0 by adding 5% of each component $p_0(i)$ to p_0, and using these n vectors as elements of the simplex in addition to p_0[1].

The algorithm then evaluates the function f at each point and order the $n+1$ vertices to satisfy

$$f(p_0) \leq f(p_1) \leq \cdots \leq f(p_n) \tag{B.4}$$

The method approximates a local optimum of a problem with n variables when the objective function varies smoothly and is unimodal. Four scalar parameters are necessary to update the simplex: coefficients of reflection (ρ), expansion (χ), contraction (γ), and shrinkage (σ). These conditions should satisfy

$$\rho > 0, \chi > 1, \chi > \rho, 0 < \gamma < 1, 0 < \sigma < 1 \tag{B.5}$$

The algorithm uses the following procedure to modify the simplex.

1. *Order.* Order the $n+1$ vertices by function value, such that $ff(p_0) \leq f(p_1) \leq \cdots \leq f(p_n)$.

[1] If $p_0(i) = 0$ then component $i = 0.00025$.

2. *Reflect.* Compute the reflection point p_r from

$$p_r = \bar{p} + \rho(\bar{p} - p_{n+1}) = (1+\rho)\bar{p} - \rho p_{n+1} \tag{B.6}$$

where $\bar{p} = \sum_{i=1}^{n} p_i/n$ represents the centroid of the n best points (i.e., all vertices except p_{n+1}. Evaluate $f_r = f(p_r)$.

If $f_1 \leq f_r < f_n$, accept the reflected point x_r and terminate the iteration.

3. *Expand.* If $f_r < f_1$, calculate the expansion point p_e,

$$p_e = \bar{p} + \chi(p_r - \bar{p}) = \bar{p} + \rho\chi(\bar{p} - p_{n+1}) = (1+\rho\chi)\bar{p} - \rho\chi p_{n+1} \tag{B.7}$$

Evaluate $f_e = f(p_e)$. If $f_e < f_r$, accept p_e and terminate the iteration; otherwise, accept p_r and terminate the iteration.

4. *Contract.* If $f_r \geq f_n$, perform a contraction between $\bar{p}$ and the better of p_{n+1} and p_r.

   (a) *Contract outside.* If $f_n \leq f_r < f_{n+1}$ (i.e., p_r is strictly better than p_{n+1}), perform an outside contraction,

$$p_c = \bar{p} + \gamma(p_r - \bar{p}) = \bar{p} + \gamma\rho(\bar{p} - p_{n+1}) = (1+\rho\gamma)\bar{p} - \rho\gamma p_{n+1} \tag{B.8}$$

   Evaluate $f_c = f(p_c)$. If $f_c \leq f_r$, accept p_c and terminate the iteration; otherwise, perform a shrink (step 5).

   (b) *Contract inside.* If $f_r \geq f_{n+1}$, perform and inside contraction,

$$p_{cc} = \bar{p} - \gamma(\bar{p} - p_{n+1}) = (1-\gamma)\bar{p} + \gamma p_{n+1} \tag{B.9}$$

   Evaluate $f_{cc} = f(x_{cc})$. If $f_c c < f_{n+1}$, accept x_{cc} and terminate the iteration; otherwise, perform a shrink (step 5).

5. *Shrink.* Evaluate f at the n points defined by

$$v_i = p_1 + \sigma(p_i - p_1), i = 2, \ldots, n+1 \tag{B.10}$$

Calculate $f(v_i)$. The unordered vertices of the simplex at the next iteration consist of $p_1, v_2, \ldots, v_{n+1}$.

Vita

Anathea Abad Pepperl was born on September 3, 1984 in Manila, Philippines, and immigrated to the United States in 1986. She graduated from Dumont High School, Dumont, New Jersey in 2001. Anathea received her Bachelor of Science in Biomedical & Electrical Engineering from Rensselaer Polytechnic Institute, Troy, NY in 2006. During her undergraduate education, she served as Secretary, President, and Leiutenant Governor for Circle K, a national community service organization. Anathea was inducted into RPI's Phalanx Honor Society in recognition of her outstanding leadership, service, and devotion to the alma mater. Her senior thesis involved a group project to design an agar phantom to study the efficacy of electrical impedance tomography for prostate cancer screening.

From 2006 to 2008, Anathea worked at the Faison School for Autism. In 2008, Anathea began attending Virginia Commonwealth University full-time, in pursuit of a graduate degree in Biomedical Engineering. She worked as a graduate research assistant for the Skin Integrity and Backrest Elevation (SIBRE) study at the VCU School of Nursing. Anathea also became involved in establishing the VCU student chapter of Engineers Without Borders, serving as their Treasurer from 2011 to 2012 and travelling to Bolivia for their first overseas project. Anathea has also served as Editor for the Virginia Academy of Science Biomedical & General Engineering Section and as Treasurer and member of the Judo Club. Anathea holds a sankyu (brown belt) in judo and a purple belt in Brazilian jiu jitsu and has competed and placed in the 2008 NAGA Virginia No-Gi division and the 2008 Virginia Open Judo Championships.

She is also proud to have competed in the first and (so far) only women's match for the Richmond Chess Boxing League.

Anathea resides in Richmond, VA with her husband Kevin and their two cats, Bleach and Earheart.